WATER RESOURCES RESEARCH, VOL. 35, NO. 2, PAGES 385–406, FEBRUARY 1999

# A model for stripping multicomponent vapor from unsaturated soil with free and trapped residual nonaqueous phase liquid

Chiu-On Ng[1] and Chiang C. Mei

Ralph M. Parsons Laboratory, Department of Civil and Environmental Engineering
Massachusetts Institute of Technology, Cambridge

David W. Ostendorf

Department of Civil and Environmental Engineering, University of Massachusetts, Amherst

**Abstract.** We present a model for the multicomponent vapor transport due to air venting in an unsaturated zone in the presence of free and trapped phases of residual nonaqueous phase liquid (NAPL). On the microscale the soil particles are assumed to form spherical aggregates with micropores filled with immobile water, trapped phases of NAPL and air. The interaggregate space is occupied with mobile air, and a thin film of free NAPL adheres on the aggregate surface. While the free NAPL can readily be in equilibrium with macropore vapor, the mass transfer from immobile phases in aggregates is rate-limited by aqueous diffusion. This model enables us to predict the vapor concentrations of various chemical species and the free NAPL saturation over the macroscale, based on the detailed understanding of the aqueous concentrations of the species and the trapped NAPL saturation within the aggregates. The model is compared favorably with some experimental data of sparging multicomponent vapor out of an intact core taken from a contaminated site. The distinctive features of multicomponent transport, clearly exhibited by the data, are further examined in the simulations of a hypothetical case of three-aromatic vapor transport under a radial flow field. It is found that while the vapor concentration of the most volatile component drops monotonically with time, those of the less volatile may rise as their mole fractions in the NAPL increase. The vapor concentration of a heavy component may have a local maximum at the evaporation front of the free NAPL. In the case of radial flow the free NAPL has two receding evaporation fronts. Condensation of the heavy component downstream of the far front causes a temporary increase of its total concentration there. With trapped NAPL and soil aggregation the macroscale transport is retarded, and the effluent concentrations end up in noticeable tailing.

## 1. Introduction

The effectiveness of soil vapor extraction (SVE), as a method to remediate an unsaturated zone contaminated with volatile organic compounds (VOC), relies on two factors: how fast the soil vapor can be removed, and how fast mass transfer into the venting stream from the other phases (i.e., aqueous phase in soil moisture, nonaqueous phase liquid (NAPL), and sorbed phase on solid grains) can occur on the microscopic scale. While the vapor transport rate is usually controlled by the pumping rate and the soil permeability, the interphase mass transfer rate depends on the distributions of the phases in the soil microstructure. It is crucial for a mathematical model of SVE to contain the essential features of the physicochemical process on the microscale, in order to bring forth the relevant parameters controlling the effects of phase exchange on the macroscopic vapor transport.

Local equilibrium is the common assumption used by many existing models for multiphase transport in unsaturated soils [e.g., *Marley and Hoag*, 1984; *Abriola and Pinder*, 1985; *Corapcioglu and Baehr*, 1987; *Baehr et al.*, 1989; *Johnson et al.*, 1990; *Kaluarachchi and Parker*, 1990; *Rathfelder et al.*, 1991; *Ho and Udell*, 1992]. Although this assumption can lead to simplification by relating concentrations of all phases with the equilibrium partition laws, the local equilibrium models often fail to account for kinetic behavior such as "tailing" and "rebound during shutdown" exhibited by effluent vapor concentrations [*Crow et al.*, 1987; *DiGiulio*, 1992]. In some other models [e.g., *Sleep and Sykes*, 1989; *Brusseau*, 1991; *Lingineni and Dhir*, 1992; *Armstrong et al.*, 1994], the interphase mass transfer rates are described by ad hoc first-order relations which nevertheless contain empirical transfer coefficients that cannot be readily estimated and may change in value over the course of venting [*Fischer et al.*, 1996].

The selective transport of constituents during the evaporation of multicomponent NAPL in unsaturated media has also received some attention. *Baehr* [1987] showed by numerical simulations that the aromatic gasoline constituents, due to higher water/air partition coefficients, dominate in the total hydrocarbon partitioned in an unsaturated zone. *Rathfelder et al.* [1991], *Lingineni and Dhir* [1992], and *Ho et al.* [1994] conducted through-flow venting experiments in laboratory-packed columns emplaced with residual multicomponent NAPL, but no residual water. In particular, *Rathfelder et al.*

[1]Now at Department of Mechanical Engineering, University of Hong Kong, Hong Kong.



Paper number 98WR02166.
0043-1397/99/98WR-02166$09.00

[1991] and *Ho et al.* [1994], both using a local equilibrium model, have been able to predict the successive rise in the effluent vapor concentration of the heavier components upon depletion of the lighter ones. The temporal and spatial variations of the liquid compositions along the column were also investigated by *Ho et al.* [1994]. They found that the individual components propagate with separate evaporation fronts which move at a speed proportional to their vapor pressure or volatility. In addition, condensation of less volatile components was also observed to occur downstream of their evaporation fronts. These experiments suggest that in the absence of water content, the NAPL can readily equilibrate with vapor in the local pores. However, *Hayden et al.* [1994] and *Wilkins et al.* [1995] found that in columns emplaced with residual NAPL and residual water the deviation of effluent concentrations from the local equilibrium values is remarkable over extended periods of venting. The NAPL-vapor phase mass transfer appears to be rate-limited in the presence of soil moisture. *Lingineni and Dhir* [1997] also studied the kinetics in NAPL evaporation rate-limited by diffusion in the liquid phase.

More recently, *Ostendorf et al.* [1997] carried out a venting experiment on an intact core taken from a site contaminated with weathered fuel. Their data clearly manifests the multicomponent effects. In particular, the vapor concentration of a heavy component may increase for some time and exhibits a maximum in the course of venting, which is in sharp contrast to the behavior of a lighter component whose concentration decreases monotonically with time, and has a smoother spatial distribution. They also obtained elution curves with appreciable tailing, a sign of departure from local equilibrium. Their findings have motivated us to develop a model which is capable of describing the vapor transport in an unsaturated medium with microscopic phase change from multicomponent residual NAPL which is not necessarily in local equilibrium with the vapor phase.

In natural unsaturated soils the NAPL is often distributed into two phases: free and trapped [*Parker and Lenhard*, 1987]. Free NAPL is a thin oil film or lens in direct contact with mobile air, while trapped NAPL are discontinuous islands of oil occluded within the water phase; both phases are immobilized by capillary forces when the NAPL saturation is reduced to the residual level. The NAPL entrapment in a two-phase system has been extensively examined. Typically, NAPL is the nonwetting phase, while water is the wetting phase. The immiscible displacement of NAPL by water always results in a fraction of the NAPL being snapped off and left behind as blobs or ganglia in the otherwise water-filled pore space [e.g., *Chatzis et al.*, 1983; *Wilson and Conrad*, 1984]. In a three-phase system the fluid distribution is much more complex and depends on the spreading coefficient of the NAPL, which is related to its interfacial tensions with the water and the gas phases [*Wilkins et al.* 1995]. A spreading NAPL which has low interfacial tensions spreads out as a thin film between the water and the gas phases, while a nonspreading NAPL exists as discontinuous lenses between them. In any case, following the order of wetability, water always occupies the smaller pores and wets the solid surface, while air fills the larger pores and NAPL forms a film between the two phases [e.g., *Leverett*, 1941; *Blunt and Scher*, 1995; *Blunt et al.*, 1995; *Zhou and Blunt*, 1997]. Microscopic evidence of NAPL films in a three-phase system has been provided by *Hayden and Voice* [1993].

Suggested by the above observations, a reasonable microscopic three-phase fluid distribution may be constructed as follows. If both water and NAPL are at their residual saturations, air is the only mobile phase and continuously occupies the larger pores (macropores). The smaller pores (micropores) are filled with immobile water, "trapped" NAPL and trapped air, where water is adjacent to solid surfaces, trapped air is in the center of the void and "trapped" NAPL is a thin film sandwiched between air and water. An entity composed of a cluster of solid particles and the immobile and trapped phases can be regarded as an aggregate with microporosity, typically with a dimension in the order of millimeters. Being either a thin film surrounding an aggregate, or a pendular ring or lens between aggregates, the "free" NAPL resides outside the micropores and is directly exposed to the mobile air. In this study we assume that the "free" NAPL is so small in saturation that it remains practically stagnant even in the presence of air flow. With this conceptual model we can now study the various interphase mass transfer processes more systematically. While the free NAPL can readily be vaporized into the macropores, mass transfer from the trapped NAPL is rate-limited by the slow diffusion in the surrounding water, as the aqueous diffusivity is smaller than the air diffusivity by at least 4 orders of magnitude. Equilibrium partitioning between trapped NAPL and mobile air is clearly not true in general. This kinetic effect on the macroscale vapor transport has however not been well-studied in the literature.

The objective of this study is to develop a kinetic model for multicomponent vapor transport due to air venting in an unsaturated zone in which both free and trapped phases of residual NAPL exist. An idealized microstructure incorporating the above features of phase distributions will be proposed in section 2. It is basically an extension of the spherical aggregate model used by *Ng and Mei* [1996a, b] for soil vapor extraction in the absence of NAPL. In this case, trapped NAPL is distributed inside, while free NAPL is spread as a thin film outside each spherical aggregate. The microscale transport, solely by aqueous diffusion, is detailed in section 3. The mass exchange between aggregates and mobile phases appears as a source term in the macroscale vapor transport equation which is deduced in section 4. In the complete problem there is coupling not only between the microscale and the macroscale transports, but also between the individual components. Normalization of the equations is then presented in section 5 in order to bring forth the dimensionless parameters pertinent in this problem. The normalization also facilitates the use of a simplified model mixture composed of a few selected components to approximate the real mixture which may contain a large number of components. In section 6 the model is tested by comparing with the data of *Ostendorf et al.* [1997]. Using a five-alkane mixture for the modeling, the agreement between prediction and data is clearly demonstrated. The simulations in section 7 are to further examine the dynamic multicomponent effects. For simplicity, vapor transport in a radial flow in an axi-symmetrical soil layer contaminated by a three-aromatic NAPL composed of benzene, toluene and o-xylene is considered. Discussions will be focused on the effects of free and trapped NAPL on the spatial and temporal variations of the component vapor and total concentrations. Mass transfer at the microscale is also examined.

## 2. Soil Microstructure and Phase Distributions

On the basis of the preceding discussions an idealized three-fluid distribution in a soil microstructure consisting of regular

packing of spherical porous aggregates is proposed. Referring to Figure 1a, inside a unit cell $\Omega'$ is a soil aggregate $\Omega'_a$ surrounded by macropore space occupied by the free NAPL $\Omega'_o$ and the mobile air $\Omega'_g$. We assume that the volume fraction of the free NAPL is so low that it spreads as a thin stagnant film on the surface of an aggregate.

The microstructure inside an aggregate is shown in a blowup in Figure 1b. All fluids in the micropores are retained by capillary forces. The solid grains $\Omega_s$ are wetted by immobile water $\Omega_w$ which in turn encloses the trapped NAPL $\Omega_o$ and the residual air $\Omega_g$. The saturation level of the trapped NAPL is also so low that it exists as a thin layer separating the water and the trapped air. Sorption of solute onto organic matters on the solid surface is also assumed to take place.

Practically, the present model is applicable to unsaturated soils well above the water table where all residual liquid phases (water, free, and trapped NAPL) are macroscopically discontinuous and their relative permeabilities are essentially zero. Therefore, in the absence of external sources, these liquid phases remain immobile even under the influence of air seepage flow. Also, the evaporation or dissolution of the free and the trapped NAPL, owing to their low saturations, will not cause effective movement of other phases. The case of multiphase flow is not considered in this paper.

The aggregate model is essentially a conceptualization for taking into consideration various transport mechanisms on the microscale, and their interaction with the macroscale. The macroscale advective diffusion of vapor in the mobile region (interaggregate pores) is effectively coupled to the microscale diffusion of solute in the immobile region (intra-aggregate pores). The assumption that the aggregates are spheres is merely to simplify the computations for the rates of phase exchange between the two regions. Ultimately, we may view that the radius of an aggregate "$a$" which is just the characteristic dimension of an immobile region is one of the few calibration parameters in the model.

For the chemical partitioning, a species which exists in the NAPL is also vaporized in air (both free and trapped), dissolved in the immobile water, and sorbed onto the solid grains. We ignore any concentration gradient in a NAPL film, because of its small thickness, in the course of phase change of its components so that it can be regarded as a locally uniform mixture at all times. In general, the NAPL saturations are functions of space and time and have to be found as part of the solution.

As two length scales will be used in this study, we shall denote the microscale (aggregate) radial coordinate by $r$ and the macroscale coordinates by $\mathbf{x}'$. All quantities depending solely on $\mathbf{x}'$ will be distinguished by primes, including the domains $\Omega'$, $\Omega'_a$, $\Omega'_o$, and $\Omega'_g$ in Figure 1.

## 3. Aqueous Diffusion in a Spherical Aggregate

Let there be $N$ components in the NAPL mixture initially. For component $i (i = 1, \cdots, N)$ we denote the mass concentration (mass per phase volume) of its vapor in trapped air by $C_{gi}(r, \mathbf{x}', t)$, aqueous phase in immobile water by $C_{wi}(r, \mathbf{x}', t)$, and separate phase in trapped NAPL by $C_{oi}(r, \mathbf{x}', t)$. The sorbed solid phase concentration, denoted by $C_{si}(r, \mathbf{x}', t)$, is the mass of chemical per mass of soil grains. The aggregate concentration (i.e., sum of mass in all phases per volume of aggregate) for a component can then be expressed as

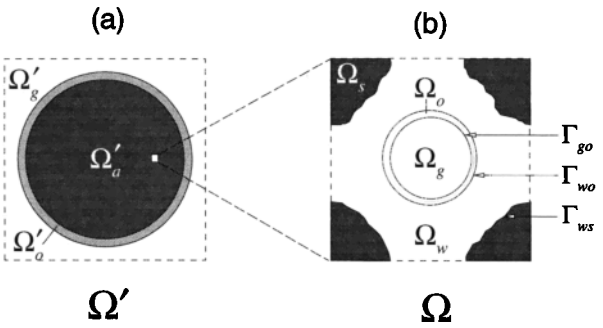


**Figure 1.** Schematic diagram of idealized microscopic fluid distributions: (a) a unit cell $\Omega'$ containing a spherical aggregate $\Omega'_a$, free NAPL $\Omega'_o$, and mobile air $\Omega'_g$; (b) a unit cell $\Omega$ inside an aggregate where $\Omega_s$ is solid grain, $\Omega_w$ is immobile water, $\Omega_o$ is trapped NAPL, and $\Omega_g$ is trapped air, $\Gamma_{go}$ is the interface between $\Omega_g$ and $\Omega_o$, $\Gamma_{wo}$ is the interface between $\Omega_w$ and $\Omega_o$, and $\Gamma_{ws}$ is the interface between $\Omega_w$ and $\Omega_s$.

$$C_{ai}(r, \mathbf{x}', t) = \phi(S_o C_{oi} + S_w C_{wi} + S_g C_{gi}) + (1 - \phi)\rho_s C_{si} \quad (1)$$
$$(i = 1, \cdots, N),$$

where $\phi$ is the volume fraction of void in an aggregate, that is, the microporosity, $\rho_s$ is the solid density, and $S_o$, $S_w$, and $S_g$ are the respective saturations (phase volume per volume of void) of trapped NAPL, water, and air in an aggregate. By definition,

$$S_o + S_w + S_g = 1. \quad (2)$$

Since water is the only connected phase within the aggregate, the mass transport inside an aggregate will solely rely on aqueous diffusion. If further a spherical aggregate of radius $a$ with radial symmetry is assumed, the aqueous diffusion can be described by

$$\frac{\partial C_{ai}}{\partial t} = \frac{1}{r^2}\frac{\partial}{\partial r}\left(r^2 \phi S_w D^*_{wi} \frac{\partial C_{wi}}{\partial r}\right) \quad (3)$$
$$0 < r < a \qquad (i = 1, \cdots, N),$$

where $t$ is the time, $r$ is the radial coordinate from the center of the sphere, and $D^*_{wi}$ is the effective aqueous diffusivity accounting for the presence of the solid grains and other phases in an aggregate. By virtue of the small length scale of the micropores, local chemical equilibrium among the various partitions is expected. Invoking the equilibrium partition laws and assuming linear sorption isotherm, we may relate the concentrations as follows:

$$C_{wi} = \gamma_i \chi_i C^{\text{sat}}_{wi}, \quad (4)$$

$$C_{gi} = \gamma_i \chi_i C^{\text{sat}}_{gi} = \gamma_i \chi_i H_i C^{\text{sat}}_{wi} = H_i C_{wi}, \quad (5)$$

$$C_{si} = K_{di} C_{wi}, \quad (6)$$

where $\gamma_i$ is the activity coefficient of component $i$ in the NAPL mixture, $C^{\text{sat}}_{wi}$ and $C^{\text{sat}}_{gi}$ are the saturation aqueous and vapor concentrations, respectively, $H_i$ is the Henry's law constant, and $K_{di}$ is the sorption partition coefficient. In addition, $\chi_i$ is the mole fraction of component $i$ in the NAPL mixture defined by

$$\chi_i = \frac{C_{oi}/M_i}{\sum_{j=1}^{N} C_{oj}/M_j} \quad (7)$$

in which $M_j$ are the molecular weights of corresponding components. Note that $C_{oi}/M_i$ is the molar concentration of component $i$ in NAPL (in units of moles per unit volume of NAPL) and that the sum of all mole fractions equals unity; that is,

$$\sum_{i=1}^{N} \chi_i = 1. \tag{8}$$

Note that the activity coefficients $\gamma_i$ become close to unity when the components have similar molecular structures [*Schwarzenbach et al.*, 1993, p. 48]. We also remark that the above equilibrium assumptions are applied locally on the microscale, over which the concentrations may still vary spatially. They therefore should not be confused with the usual assumption of local equilibrium on the macroscale, which is true only when all concentrations are uniform microscopically. For an ideal chemical mixture the total volume is equal to the sum of partial volumes of individual components:

$$\sum_{j=1}^{N} \frac{C_{oj}}{\rho_{oj}} = 1, \tag{9}$$

where $\rho_{oj}$ are the liquid densities of the pure components. By this relation we may express $C_{oi}$ explicitly in terms of $\chi_i$:

$$C_{oi} = \frac{\chi_i M_i}{\sum_{j=1}^{N} \chi_j M_j/\rho_{oj}}. \tag{10}$$

We remark that in general the aqueous and the vapor concentrations of a component are much smaller than its concentration in the NAPL. For example, from (5) and (7) we may show that on assuming unity activity coefficients,

$$C_{gi} = C_{oi} \frac{C_{gi}^{\text{sat}}/M_i}{\sum_{j=1}^{N} C_{oj}/M_j} \ll C_{oi}, \tag{11}$$

by the fact that the saturation vapor molar concentration of a component ($C_{gi}^{\text{sat}}/M_i$) is always much smaller than the molar concentration of a NAPL mixture ($\sum_{j=1}^{N} C_{oj}/M_j$). For this study, we assume that the NAPL is at a so low saturation level $S_o/S_w \ll 1$ that it forms a thin film between trapped air and immobile water.

Substituting (4)–(6) and (10) into (1), and using (11), we may write

$$C_{ai} = \phi(S_o\alpha_i + 1)\beta_i C_{wi} \qquad (i = 1, \cdots, N), \tag{12}$$

where

$$\alpha_i = \frac{M_i/(\gamma_i C_{wi}^{\text{sat}}\beta_i)}{\sum_{j=1}^{N} C_{wj}M_j/(\gamma_j C_{wj}^{\text{sat}}\rho_{oj})}, \tag{13}$$

and

$$\beta_i = S_w + (1 - S_w)H_i + (1 - \phi)K_{di}\rho_s/\phi. \tag{14}$$

Note that $\alpha_i(r, \mathbf{x}', t)$ is a function of all species concentrations $C_{wj}$, $(j = 1, \cdots, N)$, while $\beta_i$ depends only on the properties of aggregate and chemical $i$.

If the properties within an aggregate are constant, the aqueous diffusion equation (3) may now be written as

$$\frac{\partial}{\partial t}[(S_o\alpha_i + 1)C_{wi}] = \frac{S_w D_{wi}^*}{\beta_i r^2}\frac{\partial}{\partial r}\left(r^2\frac{\partial C_{wi}}{\partial r}\right) \tag{15}$$

$$0 < r < a \qquad (i = 1, \cdots, N).$$

Recall that in the presence of NAPL the aqueous concentration is governed by (4). Therefore, with (8),

$$\sum_{i=1}^{N} \frac{C_{wi}}{\gamma_i C_{wi}^{\text{sat}}} = 1 \qquad \text{for } S_o > 0. \tag{16}$$

The boundary conditions for the above diffusion equation are given by the zero flux at the center and the equilibrium partitioning on the outer surface:

$$r^2\frac{\partial C_{wi}}{\partial r}\bigg|_{r\to 0} = 0, \tag{17}$$

$$C_{wi}(r = a, \mathbf{x}', t) = C'_{gi}(\mathbf{x}', t)/H_i, \tag{18}$$

where $C'_{gi}$ is the vapor concentration in macropores for which the governing equations are to be deduced in the next section.

Equations (15)–(18) constitute the problem for the $N + 1$ unknowns: $C_{wi}(r, \mathbf{x}', t)$ where $i = 1, \cdots, N$, and $S_o(r, \mathbf{x}', t)$ which vary on both the aggregate and the macroscopic scales. With additional initial conditions they must be solved together with the vapor concentrations $C'_{gi}(\mathbf{x}', t)$ which depends on the macroscale coordinate $\mathbf{x}'$. Owing to the term $S_o\alpha_i$ on the left-hand side of (15), the transports of individual components are nonlinearly coupled with one another. The coupling disappears only when $S_o$ becomes zero throughout the aggregate, or when the NAPL is completely dissolved. When this becomes true, the aqueous concentrations are decoupled and can be found separately [*Ng and Mei*, 1996a, b]:

$$C_{wi} = \frac{C'_{gi}}{H_i} - \frac{2a}{H_i r}\sum_{n=1}^{\infty}\left\{\frac{(-1)^{n+1}}{n\pi}\sin\frac{n\pi r}{a}\int_0^t e^{-\lambda_{ni}(t-\tau)}\frac{\partial C'_{gi}}{\partial \tau}d\tau\right\}, \tag{19}$$

where

$$\lambda_{ni} = \frac{n^2\pi^2 S_w D_{wi}^*}{\beta_i a^2}. \tag{20}$$

## 4. Vapor Transport on the Macroscale

Recall that all quantities which depend on the macroscale only are distinguished by a prime. By virtue of the large air diffusivity, the vapor concentration in the free air $C'_{gi}(\mathbf{x}', t)$ is essentially uniform over a unit cell $\Omega'$; this fact can be justified by the mathematical theory of homogenization [*Ng and Mei*, 1996a]. With vapor advection and diffusion being the major transport mechanisms, the effective transport equation for component $i$ on the macroscale can be written as

$$\frac{\partial C'_{ti}}{\partial t} + \nabla'\cdot(\theta_g\mathbf{u}'C'_{gi}) - \nabla'\cdot(\theta_g D_{gi}\nabla' C'_{gi}) = 0 \tag{21}$$

$$(i = 1, \cdots, N),$$

where $\theta_g = |\Omega'_g + \Omega'_o|/|\Omega'| \sim |\Omega'_g|/|\Omega'|$ is the macroporosity, $\mathbf{u}'$ is the air seepage velocity, $D_{gi}$ is the diffusivity in the interaggregate air. The total bulk concentration $C'_{ti}(\mathbf{x}', t)$,

which equals the total concentration of component $i$ over a unit cell $\Omega'$, is given by

$$C'_{ti}(\mathbf{x}', t) = \theta_g[S'_o C'_{oi} + (1 - S'_o)C'_{gi}] + \theta_a\langle C_{ai}\rangle \quad (22)$$
$$(i = 1, \cdots, N),$$

where $S'_o(\mathbf{x}', t) = |\Omega'_o|/|\Omega'_g + \Omega'_o|$ is the free NAPL saturation in macropores, $\theta_a = |\Omega'_a|/|\Omega'| = 1 - \theta_g$ is the fraction of bulk volume occupied by aggregates, $C'_{oi}(\mathbf{x}', t)$ is the concentration in the free NAPL, and $\langle C_{ai}\rangle(\mathbf{x}', t)$ is the mean value of $C_{ai}$, defined in (12), over an aggregate $\Omega'_a$. Since the free NAPL is in the form of a thin film, chemicals within must be uniformly distributed and the equilibrium partition laws apply. Hence

$$C'_{gi} = \gamma_i \chi'_i C^{\text{sat}}_{gi}, \quad (23)$$

where

$$\chi'_i = \frac{C'_{oi}/M_i}{\sum_{j=1}^{N} C'_{oj}/M_j}. \quad (24)$$

Again, we use the volume totality relation $\sum_{j=1}^{N} C'_{oj}/\rho_{oj} = 1$ to express $C'_{oi}$ explicitly in terms of $\chi'_i$:

$$C'_{oi} = \frac{\chi'_i M_i}{\sum_{j=1}^{N} \chi'_j M_j/\rho_{oj}}, \quad (25)$$

which is similar to (10). On replacing $\chi'_i$ by using (23), we may further write

$$C'_{oi} = \alpha'_i C'_{gi}, \quad (26)$$

where

$$\alpha'_i(\mathbf{x}', t) = \frac{M_i/(\gamma_i C^{\text{sat}}_{gi})}{\sum_{j=1}^{N} C'_{gj} M_j/(\gamma_j C^{\text{sat}}_{gj}\rho_{oj})}, \quad (27)$$

which is parallel to $\alpha_i$ in the aggregate problem. The free NAPL saturation is also assumed to be much smaller than unity:

$$S'_o \ll 1. \quad (28)$$

On substituting the above relations into (21), we obtain a macroscale vapor transport equation in terms of $C'_{gi}$:

$$\theta_g \frac{\partial}{\partial t}[(S'_o\alpha'_i + 1)C'_{gi}] + \nabla' \cdot (\theta_g \mathbf{u}' C'_{gi}) - \nabla' \cdot (\theta_g D_{gi} \nabla' C'_{gi})$$
$$= -\theta_a \frac{\partial \langle C_{ai}\rangle}{\partial t} \qquad (i = 1, \cdots, N). \quad (29)$$

We remark that for aggregated soils the seepage velocity can also be found from Darcy's law, where the permeability depends on the packing of the aggregates (but not the microporosity), as has been shown formally by *Ng and Mei* [1996a].

Similar to the aggregate diffusion problem, the component concentrations are constrained by the totality condition in the presence of NAPL:

$$\sum_{i=1}^{N} \chi'_i = \sum_{i=1}^{N} \frac{C'_{gi}}{\gamma_i C^{\text{sat}}_{gi}} = 1 \qquad \text{for } S'_o > 0, \quad (30)$$

in view of (23).

In addition, initial and boundary conditions on the macroscale must be imposed (e.g., zero concentration at a large distance, and zero concentration gradient at the screen of a pumping well). Then, (29) aided by (30) define the macroscale transport problem for $N + 1$ unknowns: $C'_{gi}(\mathbf{x}', t)$ where $i = 1, \cdots, N$, and $S'_o(\mathbf{x}', t)$. Note that the two saturations $S_o$ and $S'_o$ keep track of the volume changes of the trapped and free NAPL, which are required when calculating the mass change of individual components in the separate phase. In the absence of soil aggregation the aggregate source term may be omitted; (29) reduces to the local equilibrium theory considered by *Ho et al.* [1994].

Note that in addition to the intercomponent coupling, there is also coupling between the aggregate diffusion and the macroscale transport problems. While by (18) the boundary value of $C_{wi}(r = a)$ is affected by the local value of $C'_{gi}$, the change in the total mass in aggregates is a source term for the vapor transport on the right-hand side of (29). As noted earlier, the coupling between components disappears when all NAPL phases are removed or when both $S'_o$ and $S_o$ are identically zero. If this is true, the effective vapor transport equation becomes

$$\theta_g \frac{\partial C'_{gi}}{\partial t} + \nabla' \cdot (\theta_g \mathbf{u}' C'_{gi}) - \nabla' \cdot (\theta_g D_{gi} \nabla' C'_{gi})$$
$$= -\frac{6 S_w \phi D^*_{wi} \theta_a}{a^2 H_i} \sum_{n=1}^{\infty} \int_0^t e^{-\lambda_{ni}(t-\tau)} \frac{\partial C'_{gi}}{\partial \tau} d\tau, \quad (31)$$

as has been obtained previously by *Ng and Mei* [1996a, b].

## 5. Normalization

In the present study, we shall further assume for simplicity that the soil and the initial NAPL (free and trapped) composition are homogeneous such that the soil properties $a$, $\phi$, $\theta_g$, and $D_g$, and the initial mole fractions $\chi_{i0} (i = 1, \cdots, N)$ are all constant in space. We shall also focus on the case of ideal NAPL mixing so that the activity coefficients are all equal to unity; that is, $\gamma_i = 1 (i = 1, \cdots, N)$. Initial phase equilibrium on the macroscale is also assumed so that the initial concentrations are given by

$$C'_{gi}(\mathbf{x}', t = 0) = H_i C_{wi}(0 < r < a, \mathbf{x}', t = 0) = \chi_{i0} C^{\text{sat}}_{gi}. \quad (32)$$

We now introduce the following normalized variables (distinguished by a hat):

$$(C'_{gi}, C_{wi}, C_{ai}, C'_{ti}, C'_{oi}, C_{oi})$$
$$= \chi_{i0} C^{\text{sat}}_{gi}(\hat{C}'_{gi}, \hat{C}_{wi}/H_i, \phi\beta_i\hat{C}_{ai}/H_i, \theta_g\hat{C}'_{ti}, \hat{C}'_{oi}, \beta_i\hat{C}_{oi}/H_i), \quad (33)$$
$$\nabla' = L'^{-1}\hat{\nabla}', \quad t = (L'/U')\hat{t}, \quad \mathbf{u}' = U'\hat{\mathbf{u}}', \quad r = a\hat{r}$$

where $L'$ is a characteristic macroscopic length scale and $U'$ is the characteristic air seepage velocity. Note that by the above normalization the normalized initial vapor and aqueous concentrations are always equal to unity:

$$\hat{C}'_{gi}(\hat{\mathbf{x}}', \hat{t} = 0) = \hat{C}_{wi}(0 < \hat{r} < 1, \hat{\mathbf{x}}', \hat{t} = 0) = 1. \quad (34)$$

In terms of the normalized variables the total bulk concentration (22) becomes

$$\hat{C}'_{ti}(\hat{\mathbf{x}}', \hat{t}) = (S'_o\alpha'_i + 1)\hat{C}'_{gi} + \xi_i\langle\hat{C}_{ai}\rangle \quad (i = 1, \cdots, N), \quad (35)$$

while the macroscale vapor transport equation (29) can be written as

$$\frac{\partial}{\partial \hat{t}}[(S_o'\alpha_i' + 1)\hat{C}_{gi}'] + \nabla' \cdot (\hat{\mathbf{u}}'\hat{C}_{gi}') - Pe_i^{-1}\nabla'^2\hat{C}_{gi}' = -\xi_i \frac{\partial \langle \hat{C}_{ai} \rangle}{\partial \hat{t}} \qquad (i = 1, \cdots, N), \tag{36}$$

where

$$\alpha_i'(\hat{\mathbf{x}}', \hat{t}) = \frac{M_i/C_{gi}^{sat}}{\sum_{j=1}^{N} \chi_{j0}\hat{C}_{gj}' M_j/\rho_{oj}}, \tag{37}$$

and

$$Pe_i = \frac{L'U'}{D_{gi}}, \qquad \xi_i = \frac{\phi\beta_i\theta_a}{H_i\theta_g}. \tag{38}$$

Equation (30) now reads

$$\sum_{i=1}^{N} \chi_{i0}\hat{C}_{gi}' = 1 \qquad \text{for } S_o' > 0. \tag{39}$$

Also, the normalized free NAPL concentration is

$$\hat{C}_{oi}'(\hat{\mathbf{x}}', \hat{t}) = \alpha_i'\hat{C}_{gi}'(\hat{\mathbf{x}}', \hat{t}), \tag{40}$$

so that $S_o'\hat{C}_{oi}' = S_o'\alpha_i'\hat{C}_{gi}'$, a local storage term on the left-hand side of (36), is the mass of component $i$ in free NAPL per macropore volume.

On the microscale the normalized form of the aggregate diffusion equation is

$$\frac{\partial}{\partial \hat{t}}[(S_o\alpha_i + 1)\hat{C}_{wi}] = \frac{\sigma_i}{\hat{r}^2}\frac{\partial}{\partial \hat{r}}\left(\hat{r}^2 \frac{\partial \hat{C}_{wi}}{\partial \hat{r}}\right) \qquad (i = 1, \cdots, N), \tag{41}$$

where

$$\alpha_i(\hat{r}, \hat{\mathbf{x}}', \hat{t}) = \frac{M_i/(C_{wi}^{sat}\beta_i)}{\sum_{j=1}^{N} \chi_{j0}\hat{C}_{wj} M_j/\rho_{oj}}, \tag{42}$$

and

$$\sigma_i = \frac{S_w D_{wi}^* L'}{a^2 \beta_i U'}. \tag{43}$$

The retardation factor $\beta_i$ is defined in (14). Equation (16) becomes

$$\sum_{i=1}^{N} \chi_{i0}\hat{C}_{wi} = 1 \qquad \text{for } S_o > 0, \tag{44}$$

while the boundary conditions (17) and (18) are

$$\hat{r}^2 \frac{\partial \hat{C}_{wi}}{\partial \hat{r}}\bigg|_{\hat{r}\to 0} = 0, \qquad \hat{C}_{wi}(\hat{r} = 1, \hat{\mathbf{x}}', \hat{t}) = \hat{C}_{gi}'(\hat{\mathbf{x}}', \hat{t}). \tag{45}$$

Equations (41)–(45) govern $\hat{C}_{wi}(\hat{r}, \hat{\mathbf{x}}', \hat{t})$ and $S_o(\hat{r}, \hat{\mathbf{x}}', \hat{t})$ in terms of $\hat{C}_{gi}'(\hat{\mathbf{x}}', \hat{t})$. Once solved, the normalized aggregate concentration is obtained from (12):

$$\hat{C}_{ai}(\hat{r}, \hat{\mathbf{x}}', \hat{t}) = (S_o\alpha_i + 1)\hat{C}_{wi} \qquad (i = 1, \cdots, N) \tag{46}$$

whose aggregate mean value, required to compute the source term on the right-hand side of (36), is calculated from

$$\langle \hat{C}_{ai} \rangle = 3\int_0^1 \hat{r}^2 \hat{C}_{ai}\, d\hat{r}. \tag{47}$$

The normalized trapped NAPL concentration is

$$\hat{C}_{oi}(\hat{r}, \hat{\mathbf{x}}', \hat{t}) = \alpha_i \hat{C}_{wi}(\hat{r}, \hat{\mathbf{x}}', \hat{t}), \tag{48}$$

so that $S_o\hat{C}_{oi} = S_o\alpha_i\hat{C}_{wi}$, a local storage term on the left-hand side of (41), is the mass of component $i$ in trapped NAPL per aggregate volume.

The input parameters required for a solution of the present problem include the chemical properties $C_{gi}^{sat}$, $C_{wi}^{sat}$, $M_i$, $\rho_{oi}$, and $\chi_{i0}$, and four dimensionless parameters $Pe_i$, $\xi_i$, $\sigma_i$, and $\beta_i$. The physical significance of these dimensionless parameters is as follows. Depending on the pumping rate, $Pe_i$ is the Péclet number for the significance of advection over diffusion in the macroscale vapor transport of component $i$. The parameter $\xi_i$ is a ratio of the total mass of component $i$ in an aggregate (in the absence of trapped NAPL) to the mass of the component in macropore vapor phase under equilibrium partitioning between the two regions. Generally, a larger $\xi_i$ corresponds to a greater fraction of the species to reside in aggregates, and gives rise to a higher retardation to the macroscale vapor transport. The parameter $\sigma_i$ is a ratio of timescales between the macroscopic vapor advection and the microscopic aqueous diffusion in an aggregate. It reflects the rate of mass change of a component in the immobile and the trapped phases relative to the advective transport. A higher value of $\sigma_i$ amounts to a faster response of the aggregate concentration to the vapor concentration, and vice-versa. Local equilibrium phase partitioning is a limiting case when $\sigma_i$ is much greater than unity. Finally the parameter $\beta_i$, which appears in $\alpha_i$, $\xi_i$ and $\sigma_i$, is a retardation factor to the aqueous diffusion in an aggregate due to additional partitioning in trapped vapor and sorbed phases. A higher value of $\beta_i$, because of higher $K_{di}$ for example, will result in a smaller $\sigma_i$ or slower aggregate diffusion, as well as a larger $\xi_i$ or slower macroscale vapor transport.

Note that the influence of the initial NAPL mole fractions $\chi_{i0}$ comes into the normalized problems through the summations in (37), (39), (42), and (44), merely as weighting factors in these summations. The normalized initial conditions (34) no longer depend on the mole fractions of individual components. In other words, the normalized solutions depend only on the collective, but not individual, effects of the initial mole fractions. By virtue of this, it is possible for modeling purposes to use a simplified NAPL mixture consisting of a few representative components to approximate a real mixture such as gasoline which may have a large number of components. The approximation captures the essence of the problem without excessive computation, and is necessary if comprehensive measurements for all components are not available. One must, of course, choose the representative components such that each characterizes the properties (e.g., vapor pressure, Henry's law constant) of a certain group of similar constituents in the real mixture, and has an initial mole fraction equal to the sum of those in the group. Then, individual components in the schematized mixture would represent and reflect the gross behavior of the corresponding groups of constituents in the real mixture. This kind of approximation has been adopted by, for examples, *DePaoli et al.* [1996] and *Lingineni and Dhir* [1997].

## 6. Comparison With Experiment

### 6.1. Unidirectional Through-Flow Experiment and Modeling

We first compare our model with the experimental data obtained by *Ostendorf et al.* [1997], who measured the evaporation of gasoline and diesel fuel vapors sparged out of the field soil sample in an intact core sleeve. Steam cleaned, stainless steel sleeves were driven through, with minimum disturbance, the unsaturated zone and the contaminated capillary fringe of a weathered light petroleum spill site [*Ostendorf et al.*, 1995a]. The sleeves were mounted in series in a laboratory incubator at 12.5°C and were subjected to a flow of humidified air, which sparged hydrocarbon vapors out of the contaminated source core for subsequent degradation in the biologically active mid-depth core. Along the axis of the sleeves are a number of sampling ports, so that spatial gradients of vapor concentrations can be measured, in addition to elution concentrations at the column outlet.

The contaminant is a mixture of gasoline and diesel range hydrocarbons, subjected to at least 10 years of weathering in the ground. A head space analysis of the liquid phase has identified the fractions of some 27 volatile components [*Ostendorf et al.*, 1995b]. Over 80% of the 27 compounds are alkanes, ranging from 2-methylbutane to n-decane, with less than 20% aromatics, including appreciable ethylbenzene and xylene fractions (see Table 1). About 60% by mole fraction of NAPL compounds were not individually identified.

The experimental conditions and parameters for the source core reported by *Ostendorf et al.* [1997] are summarized as follows: column length $L' = 0.81$ m, air seepage velocity $U' = 7.4 \times 10^{-5}$ m/s, total porosity $\theta = 0.34$, macroporosity $\theta_g = 0.11$, initial NAPL bulk concentration $M_o = 3.1$ kg/m$^3$, organic carbon fraction $f_{oc} = 0.001$ kg oc/kg soil, length of column with NAPL $L'_o = 0.38$ m from the bottom, solid grain density $\rho_s = 2650$ kg/m$^3$, and average NAPL density $\bar{\rho}_o = 810$ kg/m$^3$. These are all measured values. The column length was measured after extrusion, and the porosities were obtained gravimetrically. The initial NAPL bulk concentration, which includes both free and trapped phases, is based upon methylene chloride extracts of core samples from a borehole approximately 2 m apart from the one in which the source core was obtained. The results yield an integrated total mass of 1.19 kg/m$^2$ over the contaminated sleeve interval $L'_o = 0.38$ m. The organic carbon fraction was also measured from soil samples taken from nearby boreholes. We assume that the subsoil conditions do not vary significantly over the intervals of these neighboring boreholes. We stress that NAPL is present only along the interval $L'_o$ of the column.

**Table 1.** Composition of the Weathered Fuel Contaminant

| Component | Molecular Weight, g/mol | Vapor Pressure, atm, 20°C | Mole Fraction, % |
|---|---|---|---|
| 2-methylbutane | 72.2 | 0.755 | 0.0668 |
| Pentane | 72.2 | 0.556 | 0.0244 |
| 2-methylpentane*† | 86.2 | 0.225 | 0.995 |
| 3-methylpentane | 86.2 | 0.201 | 0.631 |
| Hexane | 86.2 | 0.159 | 1.25 |
| Methylcyclopentane | 84.2 | 0.144 | 0.437 |
| 2-methylhexane*† | 100 | 0.0676 | 1.58 |
| 2,3-dimethylpentane | 100 | 0.0711 | 1.51 |
| 3-methylhexane | 100 | 0.0632 | 1.02 |
| 2,2,4-trimethylpentane* | 114 | 0.0507 | 2.12 |
| Heptane | 100 | 0.0462 | 0.57 |
| Methylcyclohexane | 98.2 | 0.0474 | 0.961 |
| 2,3,4-trimethylpentane | 114 | 0.0273 | 1.17 |
| 2,3,3-trimethylpentane | 114 | 0.0274 | 0.716 |
| 2,3-dimethylhexane | 114 | 0.0234 | 2.09 |
| 2-methylheptane | 114 | 0.0203 | 1.74 |
| 3-methylheptane*† | 114 | 0.0193 | 2.53 |
| 2,2,4-trimethylhexane | 128 | 0.0142 | 0.613 |
| Octane | 114 | 0.0137 | 1.79 |
| Nonane*† | 128 | 0.00405 | 1.34 |
| Decane | 142 | 0.00129 | 1.53 |
| Ethylbenzene* | 106 | 0.00935 | 1.11 |
| p-xylene | 106 | 0.00855 | 2.45 |
| m-xylene*† | 106 | 0.00811 | 2.58 |
| o-xylene | 106 | 0.00643 | 1.62 |
| Propylbenzene | 120 | 0.00331 | 1.05 |
| Trimethylbenzene | 120 | 0.00208 | 8.35 |

From *Ostendorf et al.* [1995b].
*Component whose vapor concentration was measured in the experiment;
†Component selected to form the hypothetical mixture for the modeling.

**Table 2.** Hypothetical Mixture for Modeling of the Unidirectional Through-Flow Problem

| Component | Vapor Pressure of Compounds Being Represented, atm, 20°C | Initial Mole Fraction $\chi_{i0}$ |
|---|---|---|
| 2-methylpentane $C_6H_{14}$ | >0.1 | 0.034 |
| 2-methylhexane $C_7H_{16}$ | 0.1–0.05 | 0.062 |
| 3-methylheptane $C_8H_{18}$ | 0.05–0.01 | 0.122 |
| Nonane $C_9H_{20}$ | 0.01–0.001 (alkanes) | 0.029 |
| m-xylene $C_8H_{10}$ | 0.01–0.001 (aromatics) | 0.171 |
| Undecane $C_{11}H_{24}$ | <0.001 | 0.582 |

For the present soil aggregation model we may further calculate the following parameters: aggregate volume fraction $\theta_a = 1 - \theta_g = 0.886$, and microporosity $\phi = (\theta - \theta_g)/\theta_a = 0.25$. Also, since the core was taken near the capillary fringe, we may assume that the trapped air saturation is negligible and the water saturation in aggregates $S_w \sim 1$.

In the experiments the vapor concentrations of the following seven components were measured: 2-methylpentane, 2-methylhexane, 2,2,4-trimethylpentane, 3-methylheptane, ethylbenzene, m-xylene, and nonane. These compounds cover a range of vapor pressures and molecular weights and can represent the collective response of the volatile components, listed in Table 1, during the venting process. For modeling, we have further shortlisted the components and chosen 2-methylpentane $C_6H_{14}$, 2-methylhexane $C_7H_{16}$, 3-methylheptane $C_8H_{18}$, m-xylene $C_8H_{10}$, and nonane $C_9H_{20}$ to represent groups of compounds with different ranges of vapor pressures, as given in Table 2. M-xylene is selected as the only aromatic in the modeling mixture. Note that 2,2,4-trimethylpentane is in the same group as 2-methylhexane. The above four selected alkane components roughly represent compounds with 6, 7, 8, and 9 carbons respectively. Their initial mole fractions are equal to the sum of the mole fractions of components being represented (given in the last column in Table 1). These four components have a total mole fraction of about 40%. To make up a unity total mole fraction, we lump all the remaining less volatile components into one heavy component, undecane $C_{11}H_{24}$.

Our task is to compare the spatial and temporal variations of the component vapor concentrations generated by our model

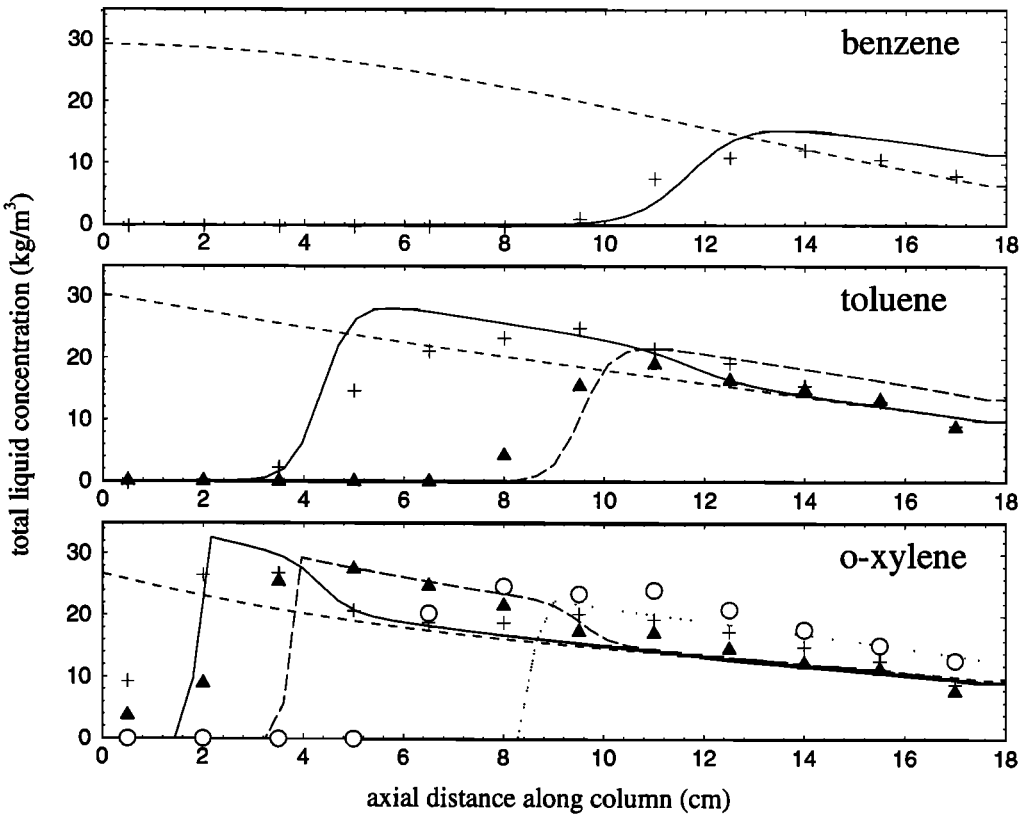


**Figure 2.** Comparison between modeling (lines) and data by *Ho et al.* [1994] (symbols) for a through-flow venting in a packed column when the venting time is 0 min (short dashes), 10 min (solid lines and crosses), 23 min (long dashes and triangles) and 48 min (dotted line and circles).

based on the five-alkane, one-aromatic mixture with the measured data. For venting in such a short column the air compressibility can be ignored, and the flow can reach a steady state readily. Equations (36) and (39) are solved for the macroscale vapor concentration and the free NAPL saturation along the column, subject to the following boundary and initial conditions:

$$\hat{C}'_{gi} - Pe_i^{-1} \frac{\partial \hat{C}'_{gi}}{\partial \hat{z}'} = 0 \qquad \hat{z}' = 0, \qquad t > 0, \tag{49}$$

$$\frac{\partial \hat{C}'_{gi}}{\partial \hat{z}'} = 0 \qquad \hat{z}' = 1, \qquad t > 0, \tag{50}$$

$$\hat{C}'_{gi} = 1 \qquad 0 < \hat{z}' < 1, \qquad t = 0, \tag{51}$$

$$S'_o = \begin{cases} S'_{o0} & 0 < \hat{z}' < 0.47, \\ 0 & 0.47 < \hat{z}' < 1, \end{cases} \qquad t = 0, \tag{52}$$

where $z'$ is the distance from the bottom of the column, $\hat{z}' = z'/L'$, and $\hat{z}' = 0.38/0.81 = 0.47$ is the initial length of the column contaminated with NAPL. The microscale diffusion problem (41)–(45) is solved with similar initial conditions:

$$\hat{C}_{wi} = 10 < \hat{r} < 1, \qquad 0 < \hat{z}' < 1, \qquad t = 0, \tag{53}$$

$$S_o = \begin{cases} S_{o0} & 0 < \hat{z}' < 0.47, \\ 0 & 0.47 < \hat{z}' < 1, \end{cases} \qquad 0 < \hat{r} < 1, \qquad t = 0. \tag{54}$$

Numerical solutions to the above problem are obtained using an alternate-direction-iterative (ADI) finite difference method, the details of which are given by *Ng* [1998]. To test our numerical scheme, we have generated results for the through-flow case presented by *Ho et al.* [1994]. In their experiments, only NAPL which is in local equilibrium with pore air is present. As shown in Figure 2, our results for the spatial and temporal changes of the three component concentrations, similar to theirs, are in good agreement with the data. We, however, obtain more abrupt evaporation fronts as 50 nodes have been used, compared to 18 nodes used by them. All our computations were executed with double precision on a Cray supercomputer. Mass balance has been checked to ensure that the numerical scheme is stable and the results are sufficiently accurate.

### 6.2. Estimation of Input Parameters for Modeling

On the basis of the above information we now evaluate the input parameters for the modeling. We first estimate the chemical properties according to the following methods.

1. Since the mixture is composed predominantly of alkanes, the activity coefficients for all components are assumed to be unity. While this may not be true for the aromatic component, m-xylene, we shall demonstrate that this component was nevertheless subject to biodegradation in the experiment.

2. The saturation vapor concentration is computed using ideal gas law, where the vapor pressure is estimated using the boiling point of the chemical [*Schwarzenbach et al.*, 1993, p. 73].

3. The solubilities $C_{wi}^{sat}$ at 25°C for the selected components are available from *Mackay and Shiu* [1981], while the boiling points and liquid densities of the components can be found from *Lide* [1996]. We estimate the temperature effect on the solubility according to [*Schwarzenbach et al.*, 1993, p. 91] log

**Table 3.** Chemical Properties and Parameters at 12.5°C for Modeling of the Unidirectional Through-Flow Problem

| Component | 2-methylpentane | 2-methylhexane | 3-methylheptane | Nonane | m-xylene | Undecane |
|---|---|---|---|---|---|---|
| $i$ | 1 | 2 | 3 | 4 | 5 | 6 |
| $M_i$, g/mol | 86.18 | 100.23 | 114.23 | 128.3 | 106.2 | 156.31 |
| $P_i^\circ$, atm | 0.1634 | 0.0473 | 0.0132 | 0.0030 | 0.0052 | 0.0003 |
| $C_{wi}^{sat}$, kg/m$^3$ | $1.4 \times 10^{-2}$ | $2.5 \times 10^{-3}$ | $7.9 \times 10^{-4}$ | $1.5 \times 10^{-4}$ | 0.16 | $4.4 \times 10^{-5}$ |
| $C_{gi}^{sat}$, kg/m$^3$ | 0.601 | 0.202 | 0.064 | 0.016 | 0.024 | 0.002 |
| $\rho_{oi}$, kg/m$^3$ | 653 | 679 | 706 | 718 | 864 | 740 |
| $H_i$ | 43 | 80 | 81 | 110 | 0.15 | 50 |
| $K_{omi}$, L/kg | $1.9 \times 10^3$ | $7.8 \times 10^3$ | $2.0 \times 10^4$ | $7.8 \times 10^4$ | 360 | $2.2 \times 10^5$ |
| $K_{di}$, L/kg | 4 | 16 | 41 | 155 | 0.7 | 448 |
| $D_{wi}^*/a^2$, s$^{-1}$ | $4 \times 10^{-4}$ | $3.7 \times 10^{-4}$ | $3.5 \times 10^{-4}$ | $3.3 \times 10^{-4}$ | $3.6 \times 10^{-4}$ | $3 \times 10^{-4}$ |
| $Pe_i$ | 190 | 190 | 190 | 190 | 190 | 190 |
| $\beta_i$ | 31 | 124 | 325 | 1235 | 7 | 3560 |
| $\xi_i$ | 1.4 | 3.0 | 7.8 | 21.9 | 88 | 139 |
| $\sigma_i$ | 0.14 | $3.3 \times 10^{-2}$ | $1.2 \times 10^{-2}$ | $2.9 \times 10^{-3}$ | 0.58 | $9 \times 10^{-4}$ |
| $\chi_{i0}$ | 0.034 | 0.062 | 0.122 | 0.029 | 0.171 | 0.582 |

$C_w^{sat} = -\Delta H_s^e/(2.303R\Theta)$ + constant, where $\Theta$ is the absolute temperature and $\Delta H_s^e$ is the aqueous enthalpy of solution which for alkanes is of the order of $-5$ kJ/mol [*Gill et al.*, 1976]. Hence it can be readily calculated that the solubility changes by a negligible amount of less than 5% when the temperature drops from 25°C to 12.5°C. The Henry's law constants are then found from the saturated vapor concentration and the solubility $H_i = C_{gi}^{sat}/C_{wi}^{sat}$.

4. Using Millington's formula [*Millington*, 1959], we estimate the effective vapor diffusivity in the pore air $D_{gi} = D_{gi}^\circ \theta_g^{7/3}/\theta^2$, where $D_{gi}^\circ$ is the vapor diffusivity in pure air. Using a typical value of $10^{-5}$ m$^2$/s for $D_{gi}^\circ$, we get $D_{gi} = 3.3 \times 10^{-7}$ m$^2$/s, from which the Péclet number $Pe_i = L'U'/D_{gi} = 190$. This value of $Pe$, which is large enough for the dominance of advection over diffusion in the transport, is used for all components.

5. The sorption partition coefficient can be expressed as the product $K_{di} = K_{omi} f_{om}$, where $K_{omi}$ is the organic matter-water partition coefficient of component $i$ and $f_{om}$ is the mass fraction of organic matter in the soil. While $f_{om}$ is approximately equal to two times $f_{oc} = 0.001$ kg oc/kg soil [*Schwarzenbach et al.*, 1993, p. 268], $K_{omi}$ can be estimated from its empirical correlation with the water solubility [*Schwarzenbach et al.*, 1993, p. 275].

So far, we have been able to estimate a priori all parameters, except the initial free and trapped NAPL saturations and $D_{wi}^*/a^2$, which are to be found by calibration. Our strategy is to assume that for small times, only the evaporation from the most volatile component, 2-methylpentane, is significant so that the component coupling effects may be ignored in this stage. We apply the vapor transport modeling for 2-methylpentane as if it were the only evaporating component; the NAPL saturations and the fractions of other components are kept to their initial values. Also, the NAPL saturations to be found are constrained by the measured value $M_o = 3.1$ kg/m$^3$ for the initial total NAPL bulk concentration, or

$$S'_{o0}\bar{\rho}_o\theta_g + S_{o0}\bar{\rho}_o\phi\theta_a = 3.1 \text{ kg/m}^3. \tag{55}$$

By curve fitting the measured spatial profiles of vapor concentration at two snapshots $\hat{t} = 10$ and 24, we have found the following calibrated values:

$$S'_{o0}(\text{calibrated}) = 0.01 \text{ (or } S_{o0} = 0.0123), \qquad \sigma_1(\text{calibrated}) = 0.14. \tag{56}$$

Because of (55), calibration of $S'_{o0}$ implies $S_{o0}$ and vice-versa, so there are only two calibrated quantities. From $\sigma_1$, we may calculate for 2-methylpentane, using (43) and (14) where $\beta_1 = 31$,

$$D_{w1}^*/a^2 = 4 \times 10^{-4}\text{s}^{-1}. \tag{57}$$

To estimate the values of $\sigma_i$ for other components, we adjust the value $D_{wi}^*$ by assuming that it is inversely proportional to the square root of the molecular weight [*Schwarzenbach et al.* 1993, p. 200].

From $S'_{o0}$ and $S_{o0}$, we calculate that the initial free and trapped NAPL concentrations, respectively, are

$$S'_{o0}\bar{\rho}_o\theta_g = 0.9 \text{ kg/m}^3, \; S_{o0}\bar{\rho}_o\phi\theta_a = 2.2 \text{ kg/m}^3. \tag{58}$$

Hence approximately 70% of the NAPL is in the trapped phase, which together with a small $\sigma_1$ in (56), suggests that macroscale transport will be appreciably rate-limited by diffusion in aggregates.

We may also use the value in (57) to estimate the order of the aggregate size. If Millington's formula is assumed to be also applicable to microporous media, and with a typical value of $D_w \sim 10^{-9}$ m$^2$/s for solute diffusion in pure water, we may find that $D_w^* \sim D_w\phi^{1/3} \sim 6.5 \times 10^{-10}$ m$^2$/s. Hence, from (57), $a \sim 1.3$ mm, which is close to the estimation of 1.4 mm by *Ostendorf et al.* [1997]. For easy reference, we summarize in Table 3 the values of chemical properties and input parameters used for the modeling of the unidirectional through-flow problem.

With the above exercise, we have illustrated a distinctive advantage of the aggregate model on describing the kinetic processes in a multicomponent chemical transport. Just based on the calibration for one component, we can readily estimate the parameters for all other components. This is in sharp contrast to a first-order kinetic model, in which the empirical transfer coefficients for individual components are not related to one another. Calibration must be carried out separately for each component, and the task would be formidable if the number of components is too large. Therefore, the amount of calibration for an aggregate model is limited and does not increase with the number of components as it does for a first-order model.

### 6.3. Results of Comparison

Using the parameters given in Table 3, we perform a simulation of the five-alkane, one-aromatic vapor transport under

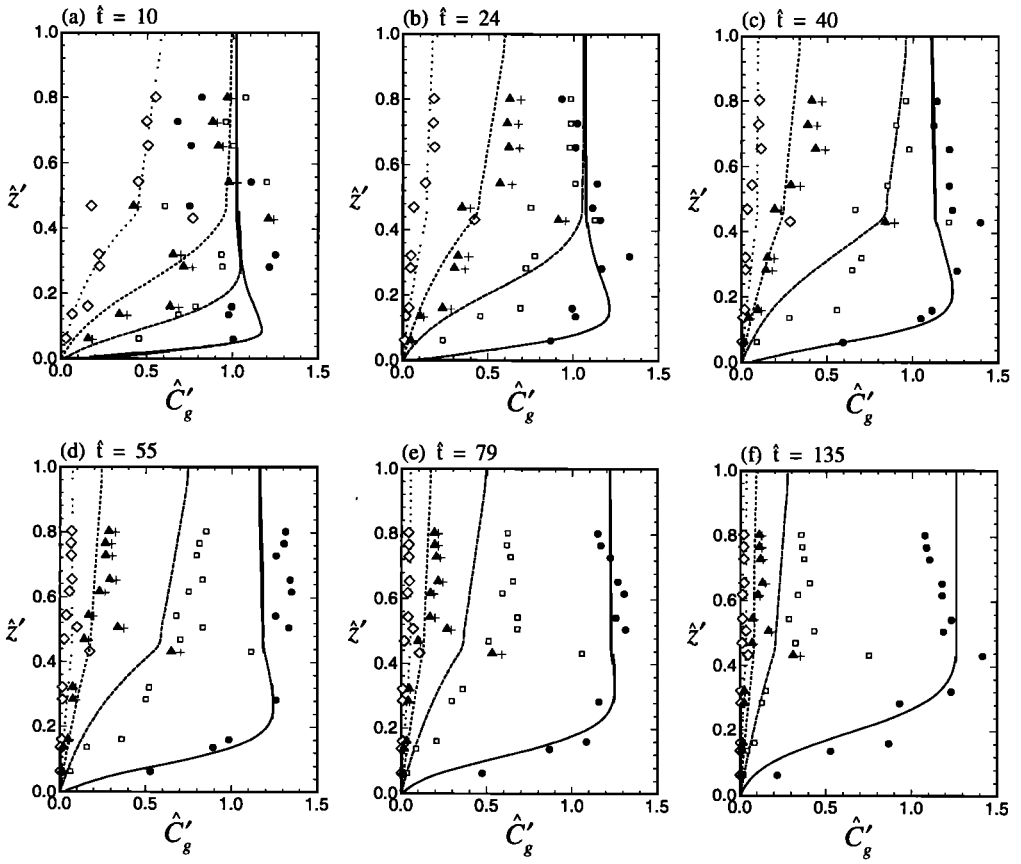


**Figure 3.** Comparison between computed (lines) and measured (symbols) vapor concentrations $\hat{C}'_g$ as a function of $\hat{z}'$ and $\hat{t}$ for 2-methylpentane (dotted lines and diamonds), 2-methylhexane (short dashes and triangles), 2,2,4-trimethylpentane (crosses), 3-methylheptane (long dashes and squares), and nonane (solid lines and circles).

the experimental conditions. It should be emphasized that the theoretical prediction is based upon rather limited calibration; just two parameters are calibrated based on concentration profiles of one component at two instants. Most of the parameters are either measured or estimated independently. The comparisons of the spatial profiles at six snap-shots of the normalized vapor concentration for 2-methylpentane, 2-methylhexane, 3-methylheptane and nonane are shown in Figure 3, while those for m-xylene are shown in Figure 4. The data points have been normalized with respect to the corresponding initial average concentrations. Only the profiles of 2-methylpentane at the first two snap-shots ($\hat{t}$ = 10, 24) have been obtained by calibration; the others are entirely prediction based on the estimated parameters. Note that the flow is moving upward and $\hat{z}'$ = 1 is the downgradient exit. From these plots we may make the following observations:

1. In each case shown in Figure 3 the prediction is in good accord with the data. Obviously the agreement is better for the two lighter components: 2-methylpentane and 2-methylhexane. Some minor discrepancies which occur at larger times for the heavier components, 3-methylheptane and nonane (Figure 3e–3f), can be ascribed to the fact that our schematized mixture may not have enough low volatility components to properly reflect their responses which become dominant in the long term. In this case, all low volatility compounds (vapor pressure less than 0.001 atm) are lumped into a single component, undecane.

2. Since 2,2,4-trimethylpentane has close properties with 2-methylhexane, we include in Figure 3 the data points (crosses) for this component as well. Clearly, when normalized, the two sets of data are indeed very close to each other. This supports the use of a component to represent similar compounds in the modeling.

3. Recall that initially the NAPL saturation drops abruptly to zero above the point $\hat{z}'$ = 0.47. At this NAPL front, a discontinuity of the vapor concentration gradient happens to all components, sooner for a lighter component. Such a gradient change appears to be confirmed by the data.

4. While the vapor concentration of the most volatile component, 2-methylpentane, decreases monotonically with time, that of nonane, except near the upstream end, rises with time so that it is greater than the initial value even at a very large time. Moreover, the predicted profiles of nonane at $\hat{t}$ = 10 – 55, supported by the data, feature a local maximum which moves slowly downgradient. Such a rise of vapor concentration with time and a local maximum in the vapor concentration distribution of a heavy component are the distinctive features of a multicomponent transport. We shall further discuss and explain these features in the next problem.

5. Figure 4 indicates a discrepancy between predicted and measured profiles for the aromatic component, m-xylene. While the predicted profiles remain essentially uniform above the NAPL source, the measured profiles decrease. We attribute the decrease to aerobic biodegradation, suppressed by

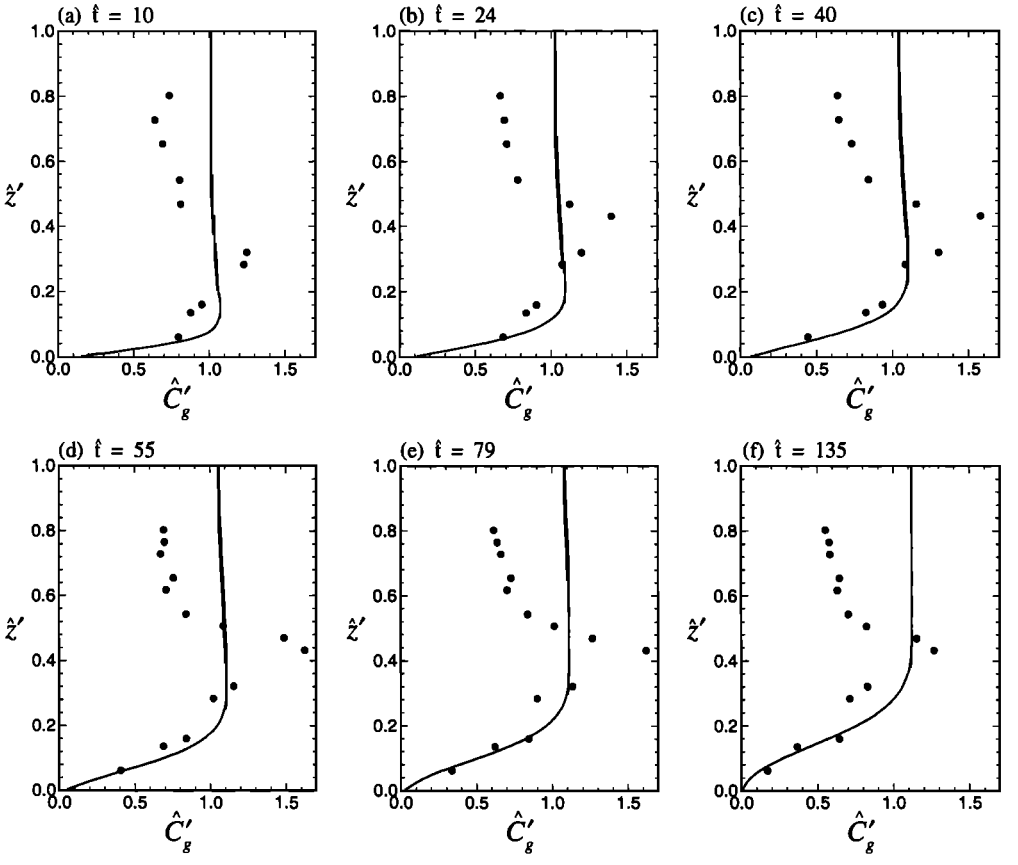


**Figure 4.** Comparison between computed (lines) and measured (circles) vapor concentrations $\hat{C}'_g$ as a function of $\hat{z}'$ and $\hat{t}$ for m-xylene.

toxicity of NAPL in the lower region of the sleeve, but active in the region above. The conclusion is further supported by aerobic microcosms taken from the site [*Ostendorf et al.*, 1997]. Peaks of m-xylene and ethylbenzene were observed on a day 1 chromatogram in the headspace of the microcosm vial containing site soil and microorganisms, as dosed with a blend of alkanes and aromatics. Two weeks later, the aromatics were gone, while the alkanes (2-methylhexane, etc) remained. We attribute the loss to biodegradation, since all compounds have roughly similar volatilities, and abiotic control soil (bugs killed in microcosm) exhibited no loss of aromatics over the same period.

Figure 5 shows the comparison of the predicted elution curves with the data for the four alkane components. For comparison, the data for 2,2,4-trimethylpentane (crosses) are also shown in the case for 2-methylhexane. Again, the close agreement in each case is demonstrated. The traits of these curves clearly reflect the volatility of the chemicals. For the most volatile component, 2-methylpentane, the evaporation takes place the fastest and the effluent concentration drops monotonically with time. For each of the moderately volatile components, 2-methylhexane and 3-methylheptane, the elution is slower and the effluent concentration drops only after a brief rise with time. The gradual diminishing of the effluent concentration, or tailing, in each of these curves is strong evidence of non-equilibrium phase exchange in the course of vapor transport, as expected from the small aggregate diffusion rates (see the small values of $\sigma_t$ in Table 3). It is also seen that the two sets of data for 2-methylhexane and 2,2,4-trimethylpentane fall very close to each other. For the less volatile component, nonane, the effluent concentration rises gradually and drops only when it reaches 26% higher than the initial value. The nonane effluent concentration remains above the initial value until after a long time of venting.

Thus far, we have shown the agreement between modeling prediction based on just two calibrated parameters and experimental data, and pointed out some of the features of a multicomponent transport. We shall further examine and explain these features in details, including changes to the NAPL saturations and microscopic mass transfer, when we study the next problem of simulating a hypothetical case of venting in a radial flow.

## 7. Simulation of a Hypothetical Venting Problem

### 7.1. Axi-Symmetrical Problem

For further illustration, we apply the present model to simulate a hypothetical problem of air venting in a horizontal soil layer with radial symmetry. The unsaturated layer, confined by impermeable top and bottom boundaries, is composed of abiotic, homogeneous and isotropic soil. Throughout the layer, the water saturation is at the residual level so that the macropore air is the only mobile phase. To simplify the computations, an idealized initial contaminant distribution is assumed. At the instant $t = 0$, a residual amount of NAPL composed of benzene, toluene and o-xylene is uniformly released into a cylindrical column of soil ($r' \leq r'_o$) where a fraction of the NAPL is trapped evenly in the aggregates while the rest re-

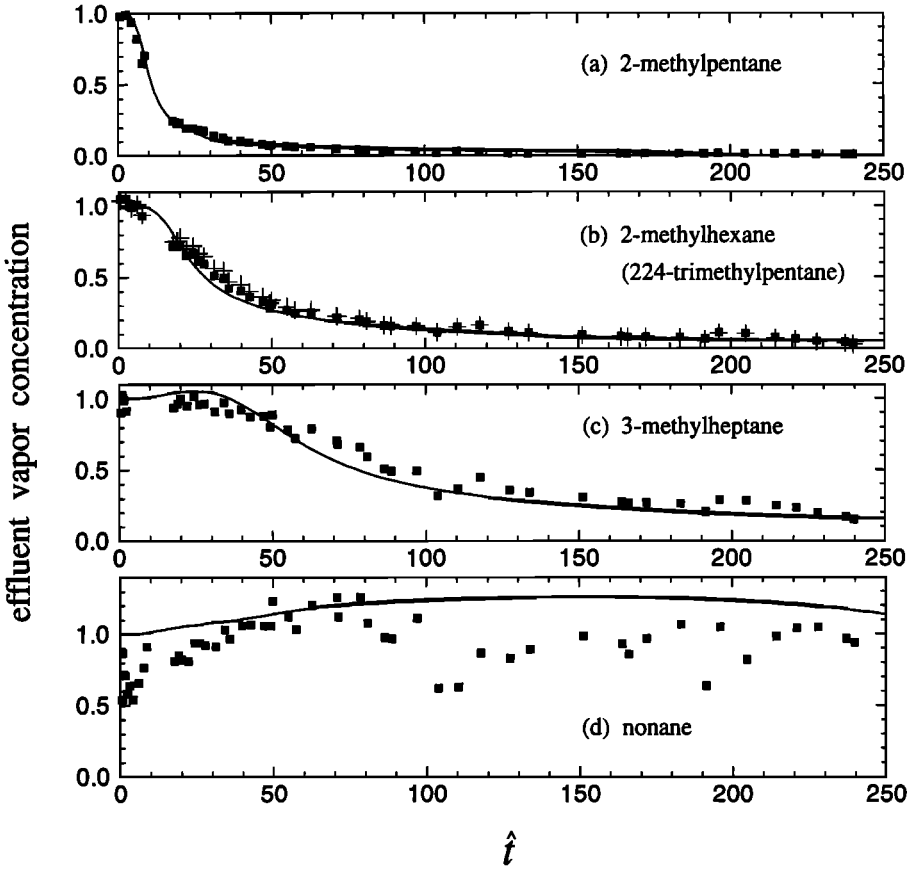


**Figure 5.** Comparison between computed (lines) and measured (squares) effluent vapor concentrations $\hat{C}'_g$ at $\hat{z}' = 1$ as a function of $\hat{t}$ for (a) 2-methylpentane, (b) 2-methylhexane, (c) 3-methylheptane, and (d) nonane. The data, denoted by crosses, for 2,2,4-trimethylpentane are included in Figure 5b for the comparison.

mains in the macropores as free phase. As NAPL continues to evaporate and dissolve locally, the macropore vapor diffuses outward to further contaminate the rest of the layer. At $t = T > 0$ a vacuum well of radius $r'_w$ is installed at the center of the column to withdraw air together with vapor from the soil. The pumping goes on until the maximum total concentrations of the components drop to a certain level. The problem is to study the effects of the NAPL, trapped and free, on the multicomponent vapor transport before and during pumping, as a function of $r'$ and $t$.

Among the three components benzene is the lightest compound, has the largest vapor pressure and is the most volatile, while o-xylene is the heaviest and the least volatile. Aromatic constituents, because of their relatively high aqueous partitions, can completely define the groundwater contaminating potential of a hydrocarbon [*Baehr*, 1987]. Total concentrations of benzene, toluene and xylene, collectively referred to as BTX, are often required by regulations to be measured to determine the contamination level of a site. All these three chemicals are spreading organics [*Demond and Lindner*, 1993; *Wilkins et al.*, 1995].

For this problem we use the diameter of the initial region of contamination as the characteristic macro length scale and define the normalized variables according to

$$\hat{r}' = r'/L', \quad \hat{u}' = u'/U', \quad \hat{p}' = p'/P_a, \quad \hat{t} = tU'/L' \tag{59}$$

where $L' = 2r'_o$, $U' = kP_a/(\theta_g L')$, $k$ is the soil permeability divided by the air dynamic viscosity, $p'$ is the soil air pressure, and $P_a$ is the atmospheric pressure. Assuming air as an ideal gas whose density varies linearly with pressure, the unsteady air flow equations for $\hat{r}' > \hat{r}'_w$, $\hat{t} > \hat{T}$ are

$$\frac{\partial \hat{p}'}{\partial \hat{t}} - \frac{1}{\hat{r}'}\frac{\partial}{\partial \hat{r}'}\left(\hat{r}'\hat{p}'\frac{\partial \hat{p}'}{\partial \hat{r}'}\right) = 0, \tag{60}$$

$$\hat{u}' = -\frac{\partial \hat{p}'}{\partial \hat{r}'}, \tag{61}$$

with the boundary conditions

$$\hat{p}' = \hat{p}'_w \qquad \hat{r}' = \hat{r}'_w, \tag{62}$$

$$\hat{p}' = 1 \qquad \hat{r}' \to \infty, \tag{63}$$

and the initial static condition

$$\hat{p}' = 1 \qquad \hat{r}'_w < \hat{r}' < \infty, \qquad \hat{t} = \hat{T}, \tag{64}$$

where $\hat{p}'_w = p'_w/P_a$ is the normalized well pressure and $\hat{T} = TU'/L'$ is the normalized period of contamination before air venting.

The macroscale vapor transport is governed by (36), in cylindrical radial coordinate, and (39), together with the following boundary and initial conditions:

$$\frac{\partial \hat{C}'_{gi}}{\partial \hat{r}'} = 0 \qquad \hat{r}' = \hat{r}'_w, \qquad \hat{t} > 0, \tag{65}$$

$$\hat{C}'_{gi} = 0 \qquad \hat{r}' \to \infty, \qquad \hat{t} > 0, \tag{66}$$

$$(\hat{C}'_{gi}, S'_o) = \begin{cases} (1, S'_{o0}) & 0 < \hat{r}' < 0.5, \\ (0, 0) & \hat{r}' > 0.5, \end{cases} \qquad \hat{t} = 0, \tag{67}$$

where $S'_{o0}$ is the initial saturation of free NAPL in macropores. The microscale aqueous diffusion is solved from (41)–(45) and the following initial conditions:

$$(\hat{C}_{wi}, S_o) = \begin{cases} (1, S_{o0}) & 0 < \hat{r}' < 0.5, \\ (0, 0) & \hat{r}' > 0.5, \end{cases} \tag{68}$$

$$0 < \hat{r} < 1, \qquad \hat{t} = 0,$$

where $S_{o0}$ is the initial saturation of trapped NAPL in micropores. The above problems are solved using a similar numerical method as that for the unidirectional through-flow problem in section 6.

To separate the effects of trapped and free NAPL, we shall consider two different types of soil to facilitate comparison:

case 1: nonaggregated soil with $\phi = 0.0$,

case 2: aggregated soil with $\phi = 0.3$ and $S_{o0} = 0.01$.

Case 1 is a special limit where the aggregates reduce to solid grains. There is no immobile water or trapped NAPL and each grain is covered by a free NAPL film which is in turn surrounded by vapor in macropore. The source term on the right-hand side of (36) vanishes, and the aggregate diffusion problem can be ignored. A similar local equilibrium problem, but with a unidirectional through-flow in a short column, has been studied by *Ho et al.* [1994]. In Case 2 there are trapped and immobile phases in the aggregates. For easy reference we summarize in Table 4 the chemical properties and other input parameters to be used in the computations. Their values are obtained as follows. The three aromatic components in the NAPL mixture are, in the order of increasing molecular weight or decreasing vapor pressure, benzene, toluene and o-xylene, of which the properties are readily found in the literature [e.g., *Perry and Green*, 1984]. As these compounds have similar molecular structures, their activity coefficients can be taken to be unity. The following parameters are chosen for all computations:

$$\hat{p}'_w = 0.5, \quad \hat{r}'_w = 0.05, \quad r'_o = 5 \text{ m}, \quad \theta_g = 0.3,$$

$$S_w = 0.7, \; S'_{o0} = 0.01, \quad \hat{T} = 100, \quad \rho_s = 2.65 \text{ kg/L},$$

$$f_{om} = 0.005, \quad k = 6 \times 10^{-10} \text{ m}^2/\text{Pa s}.$$

The fraction of organic matter, $f_{om}$, is required to calculate the sorption partition coefficient $K_{di} = K_{omi} f_{om}$ where $K_{omi}$ is the organic matter-water partition coefficient which can be estimated with the chemical's water solubility [*Schwarzenbach et al.*, 1993, p. 274]. Adopting Millington formula [*Millington*, 1959], the effective gas diffusivity can be estimated from

$$D_{gi} = D^\circ_{gi} \theta_g^{7/3} / (\theta_g + \phi \theta_a)^2 = 0.23 D^\circ_{gi} \tag{69}$$

where $D^\circ_{gi}$ is the diffusivity of the component vapor in pure air. For the present three components, the values of $D^\circ_{gi}$ are obtainable from *Fuller et al.* [1965]. For the aqueous diffusivities, we first assume that $D^*_{w1}/a^2$ is equal to $10^{-7}$ s$^{-1}$. Then $D^*_{w2}/a^2$ and $D^*_{w3}/a^2$ are estimated by assuming that the diffusion coefficient is inversely proportional the square of the molecular weight. Having established the values of these site and material properties, the dimensionless parameters $Pe_i$, $\beta_i$, $\xi_i$, and $\sigma_i$ can then be computed accordingly. Finally an initial NAPL composition of equal mole fractions ($\chi_{10} = \chi_{20} = \chi_{30} = 1/3$) of the three components is assumed.

**Table 4.** Chemical Properties and Parameters at 20°C for Modeling of the Radial Flow Problem

| Component | Benzene | Toluene | o-xylene |
|---|---|---|---|
| $i$ | 1 | 2 | 3 |
| $M_i$, g/mol | 78.11 | 92.14 | 106.17 |
| $C^{sat}_{wi}$, kg/m$^3$ | 1.34 | 0.40 | 0.13 |
| $C^{sat}_{gi}$, kg/m$^3$ | 0.32 | 0.11 | 0.029 |
| $\rho_{oi}$, kg/m$^3$ | 876 | 865 | 876 |
| $H_i$ | 0.24 | 0.28 | 0.22 |
| $K_{omi}$, $L_{water}/kg_{om}$ | 47 | 134 | 336 |
| $K_{di}$, $L_{water}/kg_{solid}$ | 0.235 | 0.67 | 1.68 |
| $D^\circ_{gi}$, m$^2$/s | $8.8 \times 10^{-6}$ | $7.9 \times 10^{-6}$ | $7.2 \times 10^{-6}$ |
| $D_{gi}$, m$^2$/s | $2 \times 10^{-6}$ | $1.8 \times 10^{-6}$ | $1.7 \times 10^{-6}$ |
| $D^*_{wi}/a^2$, s$^{-1}$ | $1 \times 10^{-7}$ | $9.2 \times 10^{-8}$ | $8.6 \times 10^{-8}$ |
| $Pe_i$ | 100 | 110 | 121 |
| $\beta_i$ | 2.22 | 4.94 | 11.17 |
| $\xi_i$ (case 1) | 0.0 | 0.0 | 0.0 |
| $\xi_i$ (case 2) | 6.48 | 12.35 | 35.53 |
| $\sigma_i$ | 0.0157 | 0.0065 | 0.0027 |
| $\chi_{i0}$ | 0.3333 | 0.3333 | 0.3333 |

From the above parameters, we can also estimate from (59) that the length and velocity scales are $L' = 10$ m, $U' = 2 \times 10^{-5}$ m/s, and therefore the timescale for the macroscale vapor transport is $L'/U' = 5 \times 10^5$ s ~6 days. The contamination period prior to pumping is $\hat{T} = 100$ which roughly corresponds to a period of 1.5 years.

### 7.2. Case 1: Nonaggregated Soil With Free NAPL Only

We first consider the case of nonaggregated soil (i.e., no micropores or trapped phases), with a view to studying the effects of free NAPL alone on the vapor transport in a radial flow field. The vapor concentrations $\chi_{i0}\hat{C}'_{gi}$ and the total bulk concentrations $\chi_{i0}\hat{C}'_{ti}$ for the three components are plotted respectively in Figures 6 and 7 as functions of $\hat{r}'$ and $\hat{t}$. The initial distributions are shown by the dashed lines which are discontinuous at the outer edge $\hat{r}' = 0.5$. Subsequent profiles of $\hat{C}'_{ti}$ are also discontinuous at this location because free NAPL saturation drops abruptly there. In the period $0 < \hat{t} < 100$, there is no air flow and the vapors diffuse radially outward. From $\hat{t} = 100$ onward, air flow is induced by a suction well at the center with a screen radius $\hat{r}'_w = 0.05$. From these plots the following observations can be made:

1. As expected, the clean-up time is longer for a less volatile component. While benzene is mostly removed at $\hat{t} = 150$, toluene is not purged until after $\hat{t} = 175$ and o-xylene is still abundant at $\hat{t} = 225$.

2. The three components exhibit different spatial and temporal variations of vapor concentration (Figure 6). For benzene and toluene the vapor concentrations have smooth spatial distributions at all times. The benzene vapor concentration decreases monotonically with time, while over much of the spill site the toluene vapor concentration rises briefly before decaying. Meanwhile, the o-xylene vapor concentration profiles exhibit two local sharp peaks which rise while moving towards each other. Concentrations between the two peaks increase with time to approach unity which corresponds to the vapor concentration in equilibrium with pure o-xylene liquid. The above behavior can be more readily understood if we also examine the spatial and temporal variations of the free NAPL saturation $S'_o$ as shown in Figure 8. Clearly, the region between

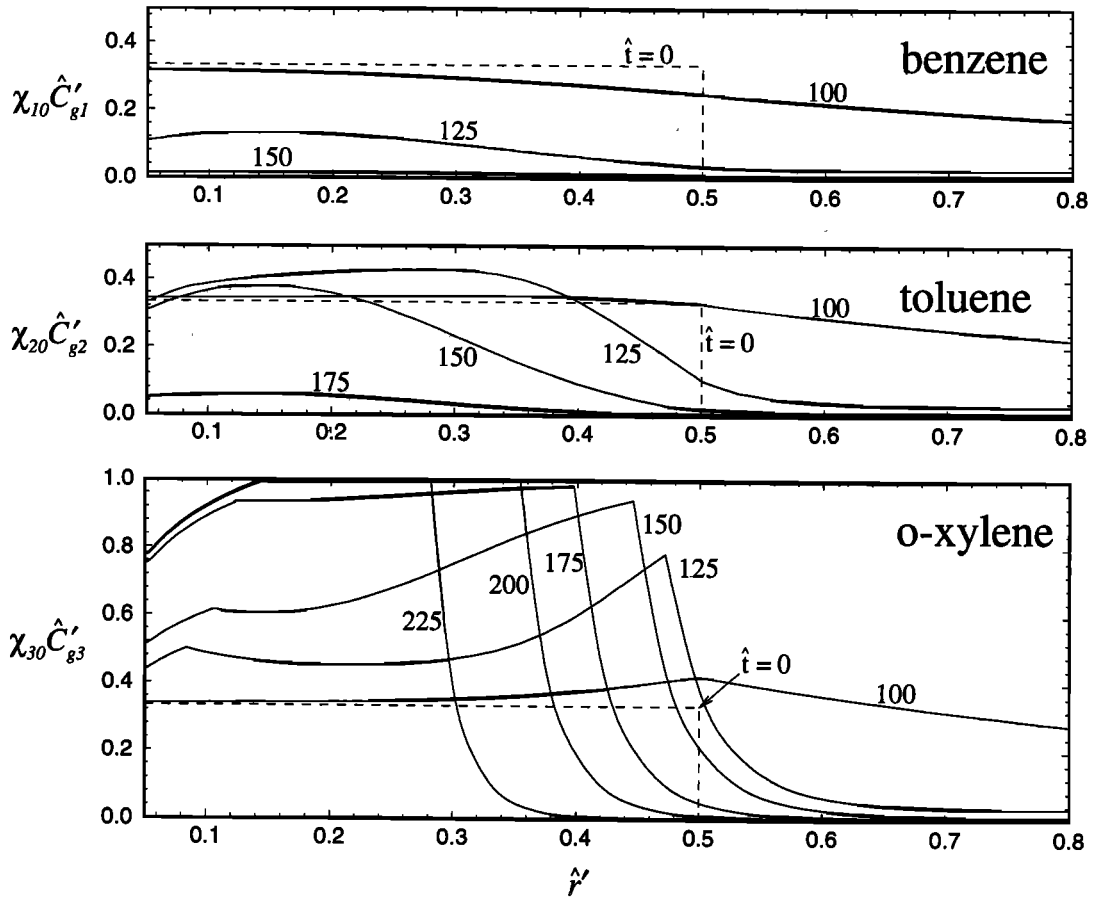


**Figure 6.** Macrospatial and temporal variations of the three-component vapor concentrations $\chi_{i0}\hat{C}'_{gi}$ for case 1. The dashes denote the initial distributions.

the two peaks correspond to where the NAPL saturation is nonzero. The NAPL has two evaporation fronts: one near the well (the near front) where the flow velocity is higher, and the other at the upstream (the far front) which is blown with clean air drawn from afar. As long as the local NAPL saturation is nonzero, the normalized vapor concentrations are given by the mole fractions of the components in the NAPL, the sum of which is fixed to be unity. Each component is however evaporated at a different rate determined by its volatility. When the lightest component is being removed from the NAPL, its mole fraction drops while those of the others increase. This explains the momentary increase of the toluene vapor concentration before benzene is largely volatilized. Eventually when toluene is also volatilized, the o-xylene vapor concentration becomes unity and the NAPL becomes virtually a pure liquid phase of o-xylene. This so-called "selective evaporation" always happens to a greater extent at the two fronts. In particular, the NAPL at the far front is always the most concentrated in o-xylene in the course of venting. All the NAPL has become virtually pure o-xylene at $\hat{t} = 200$ when its maximum saturation is reduced to 40% of the initial value. The maximum o-xylene vapor concentration is then close to unity until the whole distribution drops rapidly to zero soon after the NAPL is completely wiped out at about $\hat{t} = 250$. These component interaction effects are qualitatively consistent with our earlier observations when studying the unidirectional through-flow problem. Evaporation fronts of individual components were also found in the column tests by *Ho et al.* [1994] (see Figure 2).

3. The sharp change in gradient across the two fronts in the o-xylene vapor concentration distributions is related to the abrupt vanishing of NAPL saturation at these two locations and does not suggest numerical inaccuracy. To check this point, a simple local analysis can be carried out as follows. Suppose near the far front the NAPL saturation profile can be approximated by a jump

$$S'_o(\hat{r}', \hat{t}) \sim S'^{-}_o H[\hat{r}'_e(\hat{t}) - \hat{r}'] \tag{70}$$

where $S'^{-}_o$ is the jump value, H is the Heaviside step function, and $\hat{r}'_e(\hat{t})$ is the current position of the front. On substituting (70) into (36) which is then integrated with respect to $\hat{r}'$ across the discontinuity at $\hat{r}' = \hat{r}'_e$, we can obtain

$$\frac{d\hat{r}'_e}{d\hat{t}} = \frac{\partial \hat{C}'_{gi}}{\partial \hat{r}'}\bigg|_{\hat{r}'=\hat{r}'^{-}_e}^{\hat{r}'=\hat{r}'^{+}_e} (Pe_i S'^{-}_o \alpha'_i \hat{C}'_{gi})^{-1} \qquad \text{at } \hat{r}' = \hat{r}'_e. \tag{71}$$

Clearly, the receding speed of the evaporation front is directly proportional to the change in vapor concentration gradient across the front. To verify the above relationship, we have compared the speed of the evaporation front obtained by numerically keeping track of the position of the front as a function of time, and that computed directly from (71). The two results are found in very good agreement [*Ng*, 1998]. It is also found that the front is moving at an almost steady speed until it suddenly speeds up tremendously just before the NAPL is completely evaporated.

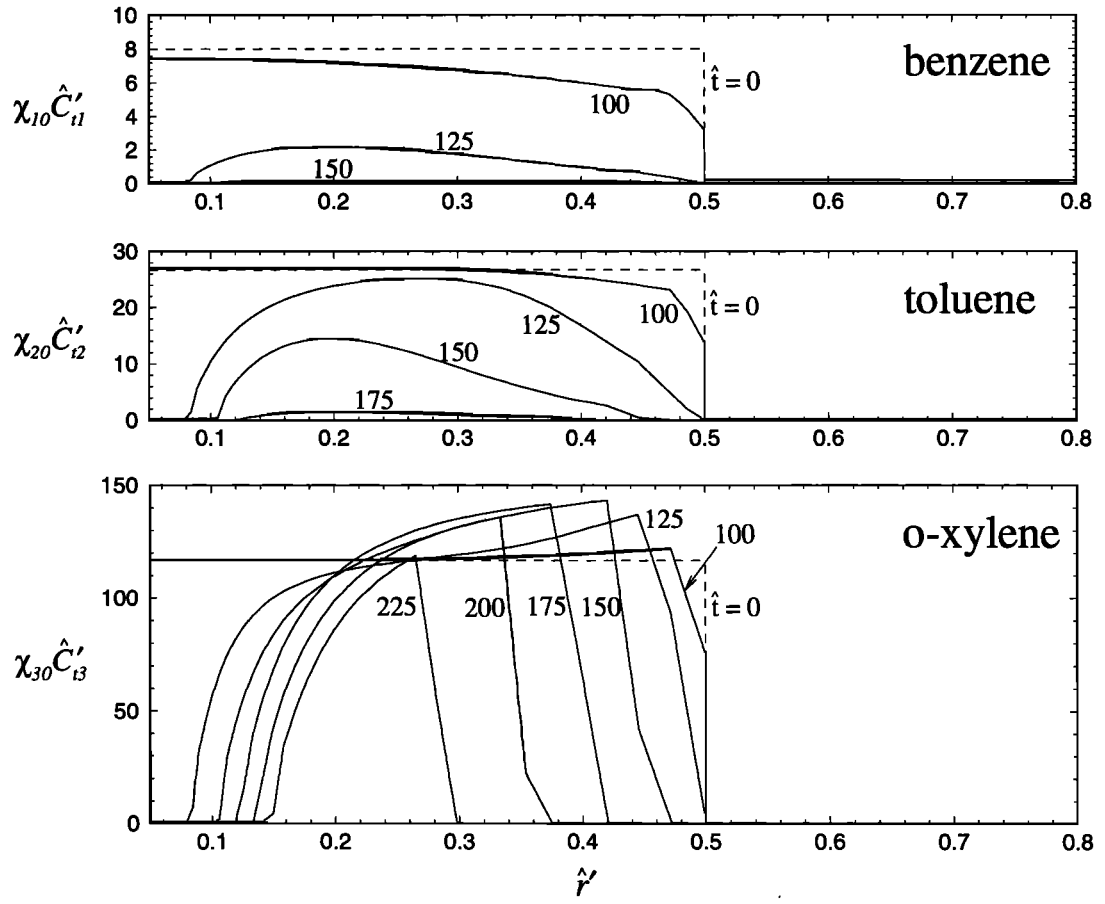


**Figure 7.** Macrospatial and temporal variations of the three component total concentrations $\chi_{i0}\hat{C}'_{ti}$ for case 1. The dashes denote the initial distributions.

4. The total concentration $\hat{C}'_{ti}$ is dominated by the mass of free NAPL per bulk volume; it becomes relatively small when the free NAPL is volatilized (Figure 7). For benzene and toluene the smooth distributions of the total concentrations decrease monotonically as pumping continues. However, for o-xylene the total concentration, or free NAPL concentration, immediately downstream of the far front (the peak) rises above the initial value for most of the time (see $\hat{t}$ = 100–200 curves for o-xylene in Figure 7). Since NAPL is an immobile phase, any local increase in mass of NAPL can only be brought about by "condensation" of vapor phase. The rationale for the condensation of o-xylene vapor into NAPL can be explained as follows. At the far front, the o-xylene vapor concentration is always the maximum and therefore has a positive downstream gradient (see the o-xylene curves in Figure 6). Advection of vapor toward the well causes a net increase of vapor concen-

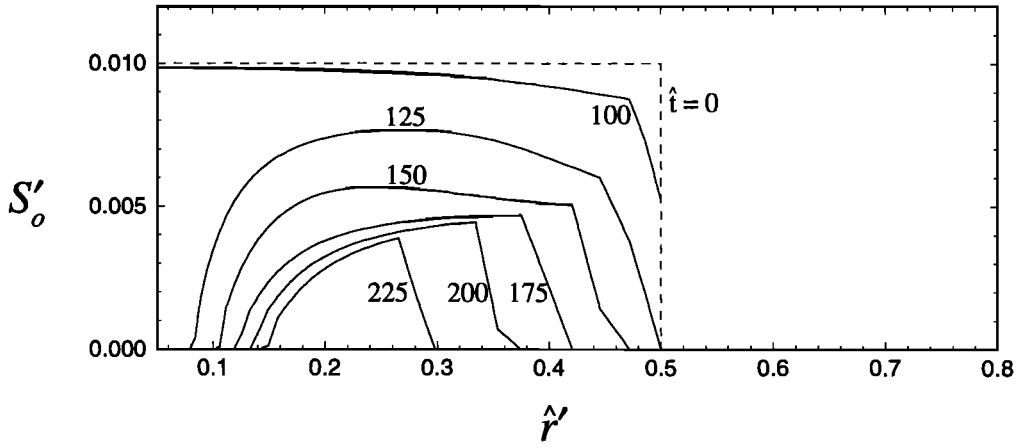


**Figure 8.** Macrospatial and temporal variations of the free NAPL saturation $S'_o$ for case 1. The dashes denote the initial distribution.

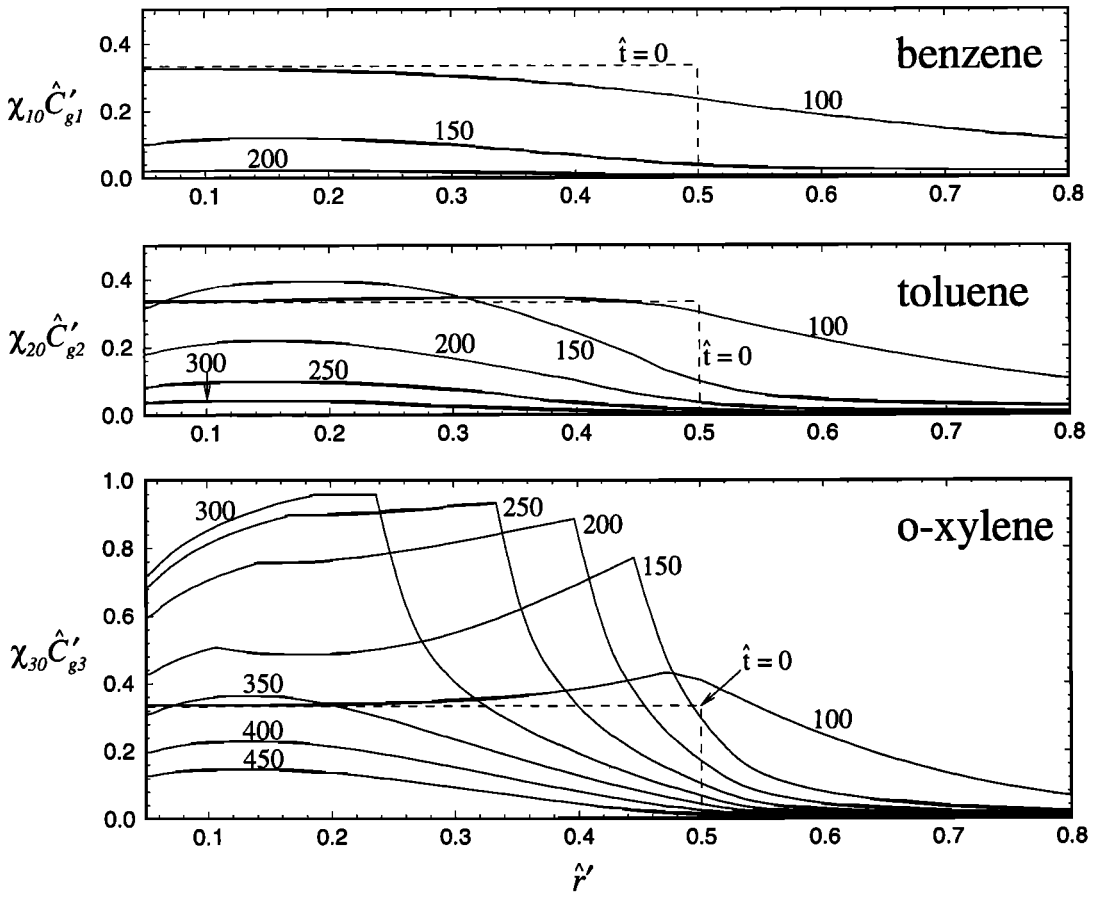


**Figure 9.** Macrospatial and temporal variations of the three-component vapor concentrations $\chi_{i0}\hat{C}'_{gi}$ for case 2. The dashes denote the initial distributions.

tration in downstream pores already filled with o-xylene vapor in equilibrium with the liquid phase. The phase equilibrium between vapor and NAPL can be restored only after the extra amount of vapor is condensed into liquid to give a higher mole fraction of o-xylene in the NAPL mixture. The condensation process stops only when the positive vapor concentration gradient diminishes. Such condensation of heavier components downstream of an evaporation front was also observed in the column experiments by *Ho et al.* [1994].

### 7.3. Case 2: Aggregated Soil With Trapped NAPL

In this case we focus on the additional effects of immobile water and trapped NAPL in an aggregated soil. Let us first examine the macroscopic transport behavior.

**7.3.1. Macroscale variations.** The vapor concentrations $\chi_{i0}\hat{C}'_{gi}$ and the total bulk concentrations $\chi_{i0}\hat{C}'_{ti}$ for the three components, and the NAPL saturations for free and trapped phases are plotted respectively in Figures 9, 10, and 12 as functions of $\hat{r}'$ and $\hat{t}$. Again, the initial distributions are shown by the dashed lines which are discontinuous at the outer edge $\hat{r}' = 0.5$. Subsequent profiles of $\hat{C}'_{ti}$ and $\langle \hat{C}_{ai} \rangle$ are also discontinuous at this location because the NAPL saturations drop abruptly there. Features from these plots can be summarized as below:

1. The pumping time required to clean up each component is prolonged by the presence of the immobile and trapped phases. As compared to case 1, the clean-up time lengthens more for heavier components, ranging from two times for benzene to over three times for o-xylene (see Figure 9).

2. As in case 1, the o-xylene vapor concentration exhibits an increase with time, approaching unity, in the free NAPL region (where the free NAPL saturation is nonzero). However, the vapor concentration drops more slowly than case 1 after the free NAPL at that position is volatilized. This is because even in the absence of free NAPL the aggregates are still producing vapor into the macropores. As a result, the o-xylene vapor concentration decays only gradually with a smooth profile after the free NAPL is completely volatilized (see Figure 9 for $\hat{t} > 300$).

3. The total concentration is dominated by the mass of free NAPL and the mass in aggregates per bulk volume. As in case 1, but at a slower rate, the total concentrations of benzene and toluene decrease monotonically with time while that of o-xylene features an increase as the peak vapor concentration is being advected downstream (see Figure 10). Such increase in total concentration is again caused by a net influx of vapor associated with a positive concentration gradient. In this case, the additional mass is partly condensed to free NAPL (as the peaks on the o-xylene curves $\hat{t} = 100$–$250$ in Figure 11a are higher than the initial value), and partly transferred into storage in aggregates (as the top parts of the o-xylene curves $\hat{t} = 100$–$300$ in Figure 11b are higher than the initial value). See also the next paragraph for a microscopic reasoning. The free NAPL region is distinguishable, being the more concave part

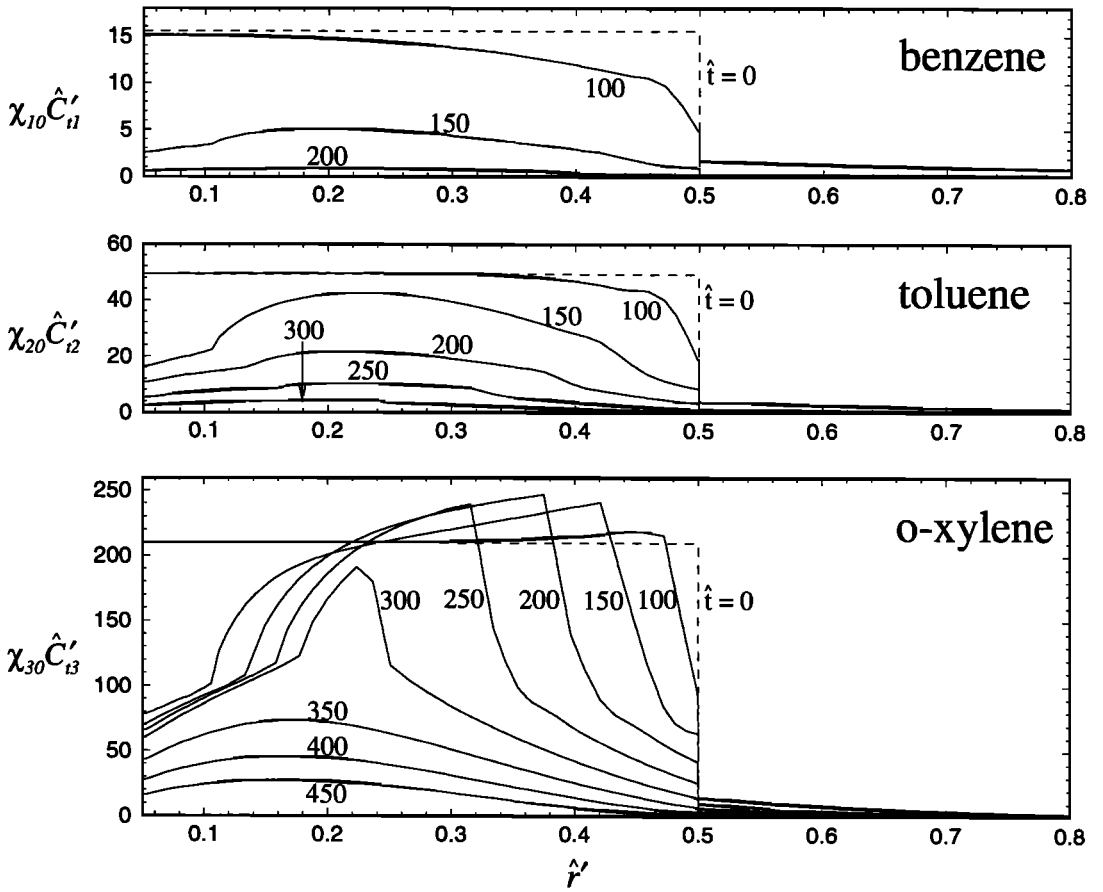


**Figure 10.** Macrospatial and temporal variations of the three-component total concentrations $\chi_{i0}\hat{C}'_{ti}$ for case 2. The dashes denote the initial distributions. The profiles for $\hat{r}' > 0.5$ diminish monotonically from $\hat{t} = 100$ onward.

in an o-xylene total concentration profile (compare the o-xylene concentration profiles in Figures 10 and 11a and the free NAPL saturation distributions in Figure 12a). Again, the total concentration decays slowly, and its distribution becomes smooth after the free NAPL is completely volatilized (see Figure 10).

4. In the presence of aggregates, the volatilization of the free NAPL is retarded, by a factor over 30% in this example. The free NAPL $S'_o$ has two abrupt evaporation fronts, and is completely volatilized much sooner than the trapped NAPL (see Figure 12a). In the presence of free NAPL the mean trapped NAPL saturation $\langle S_o \rangle$ has an approximately uniform distribution which drops slower than where the free NAPL is gone (see Figure 12b). However, the trapped NAPL saturation is not completely purged even long after the free NAPL has vanished (see the next paragraph).

**7.3.2. Microscale variations.** To gain further insight, it is also of interest to examine how mass transfer of each component takes place within an aggregate. Figures 13 and 14 show, respectively, the microscopic distributions of the aqueous concentrations and the trapped NAPL saturation in an aggregate at the macroscale position $\hat{r}' = 0.25$ (i.e., in the middle of the spill zone). For benzene the aqueous concentration decreases monotonically with time, implying a constant depletion of this most volatile component from the aggregate. Toluene is first fed into and then removed from the aggregate, in response to the increase and then decrease in macropore vapor concentration here. The feeding of o-xylene into the aggregate lasts even longer and results in a more pronounced increase in the o-xylene aqueous concentration. Therefore, while the lighter components are being removed from the aggregate, more of the heaviest component is being stored in the aggregate (the macrospatial increase in the aggregate storage of o-xylene where free NAPL is present is clearly shown in Figure 11b). This trend stops only when the macropore o-xylene vapor concentration begins to drop, or when the free NAPL saturation at this macroscale position vanishes. This happens around $\hat{t} = 300$ for $\hat{r}' = 0.25$ (see Figures 11a and 12a). After this moment, the trapped NAPL saturation profile exhibits a front which retreats as NAPL dissolution goes on (Figure 14). The o-xylene aqueous concentration has a discontinuous gradient across this front. In the outer region o-xylene diffuses outward, while in the inner region the o-xylene aqueous concentration continues to rise to approach unity, as the trapped NAPL becomes purer in o-xylene (Figure 13). Note that the trapped NAPL is not completely removed even at a large time; its rate of disappearance decreases as it is more confined to the center of the aggregate (Figure 14). The NAPL trapped at the core of an aggregate requires a very long time to be removed.

**7.3.3. Effluent vapor concentration.** Finally, let us compare the effluent vapor concentrations for the three components that can be measured at the pumping well, for cases 1 and 2 (Figure 15). In either case, the benzene concentration decreases monotonically with time, while the toluene concen-

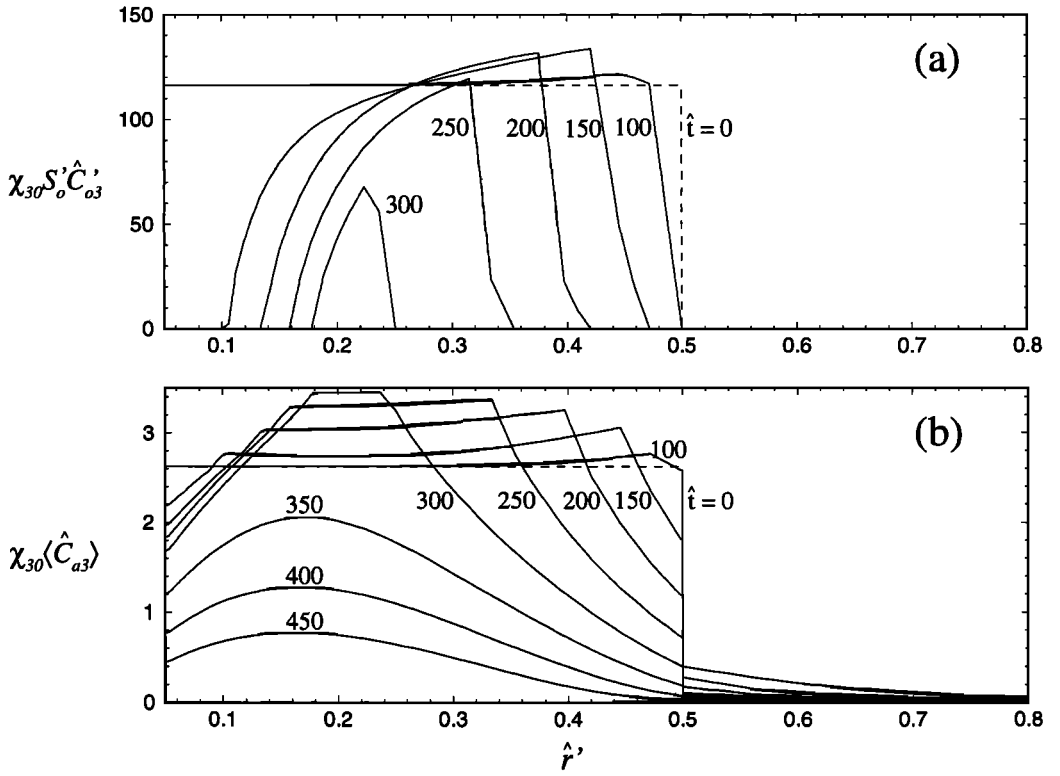


**Figure 11.** Macrospatial and temporal variations of o-xylene concentrations in (a) free NAPL (mass per macropore volume) $\chi_{30}S'_o\hat{C}'_{g3}$, and (b) aggregate (total mass of trapped NAPL, aqueous, and sorbed phases per aggregate volume) $\chi_{30}\langle\hat{C}_{a3}\rangle$, both for case 2. The dashes denote the initial distributions. The profiles for $\hat{r}' > 0.5$ diminish monotonically from $\hat{t} = 100$ onward.

tration first drops and then rises briefly before it drops back. The change for the o-xylene concentration is more dramatic. After the initial rise, it drops momentarily as the free NAPL near the well is volatilized. This is followed by a pronounced increase to more than twice the initial value until the free NAPL is completely volatilized. In case 1 where the aggregate effects are absent, the o-xylene concentration finally drops abruptly all the way down to zero. However, with trapped NAPL, the final drop in case 2 is much milder; it ends up in a tail where the effluent concentration decays at a persistently slow rate. In fact, the effluent tailing is characteristic for all transports with nonequilibrium phase exchange on the macroscale. Obviously, the trapped phases in aggregates retard the removal of all components, more for the heavier than the lighter ones. The results in case 2 are qualitatively similar to the elution curves (Figure 5) obtained for the unidirectional through-flow problem.

The elution curves can be useful in calibrating the free NAPL saturation. Very often only the total NAPL saturation can be measured readily in practice. As discussed above, the time at which the effluent concentration of the heaviest component drops abruptly is the time when the free NAPL is completely volatilized, and therefore can be used to calibrate the amount of free NAPL present in the soil. If the total NAPL saturation is known, the trapped NAPL saturation can then be found from their difference. If not, the decaying speed of the tailing, which depends on the amount of trapped NAPL in aggregates, can be used to calibrate the trapped NAPL saturation.

## 8. Concluding Remarks

On the basis of the spherical aggregate diffusion model we have presented a multicomponent vapor transport theory for soil vapor extraction in unsaturated soils with mass exchange kinetics due to free and trapped phases of residual NAPL. The assumptions are that the free NAPL is in direct contact with the mobile air, and the trapped NAPL together with aqueous, sorbed, and trapped vapor phases are distributed inside the aggregates. While local equilibrium between the "free" NAPL and the macropore vapor is readily attained, the mass transfer between the "trapped" phases and the macropore vapor is rate-limited by aqueous diffusion. Equations (15)–(18) govern the aqueous diffusion and the trapped NAPL saturation in a microscale aggregate, while equations (29)–(30) are for the vapor transport and the free NAPL saturation on the macroscale. Through mass exchange between phases, the two problems are coupled to each other. Individual components also interact with one-another in the transport as long as they are tied by the totality condition of mole fractions in the presence of NAPL. The normalized problems are expressible in terms of four dimensionless parameters which are functions of flow, soil and chemical properties. The normalization also facilitates, for comparing modeling and data, the use of a hypothetical mixture composed of a few representative components to approximate a real mixture of more complex composition, when comprehensive measurements for all components are not available.

We have compared the present theory with experimental data obtained from a venting of multicomponent vapor in an

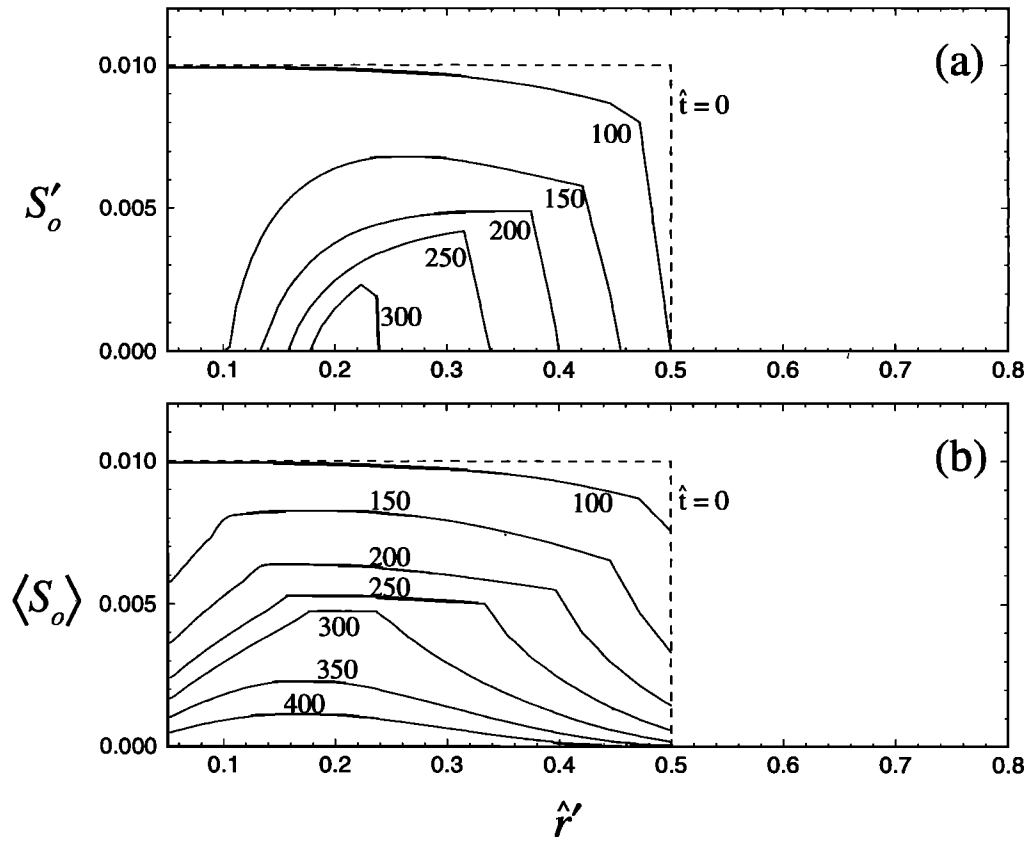


**Figure 12.** Macrospatial and temporal variations of (a) the free NAPL saturation $S'_o$ and (b) the mean trapped NAPL saturation $\langle S_o \rangle$ for case 2. The dashes denote the initial distributions.

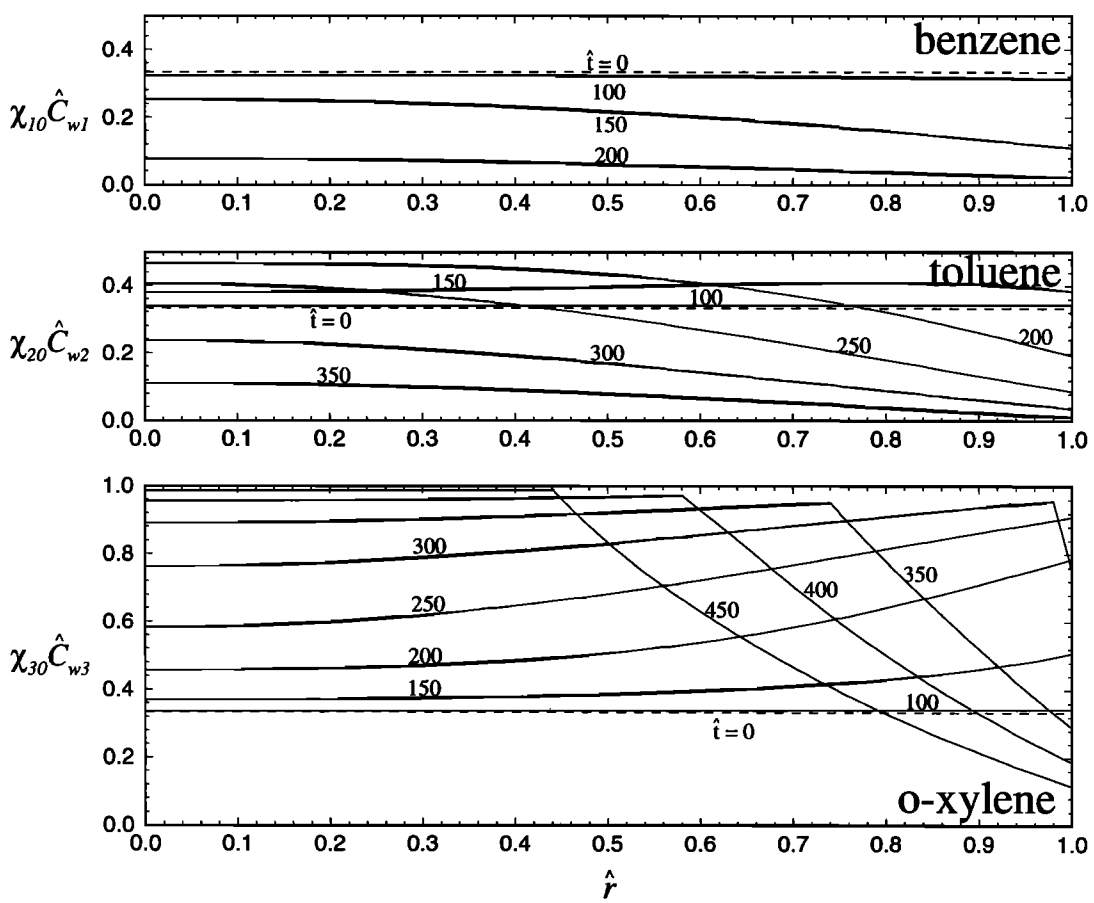


**Figure 13.** Microspatial and temporal variations of the component aqueous concentrations $\chi_{i0}\hat{C}_{wi}$, at the macroposition $\hat{r}' = 0.25$ (middle of spill site) for case 2. The dashes denote the initial distributions.

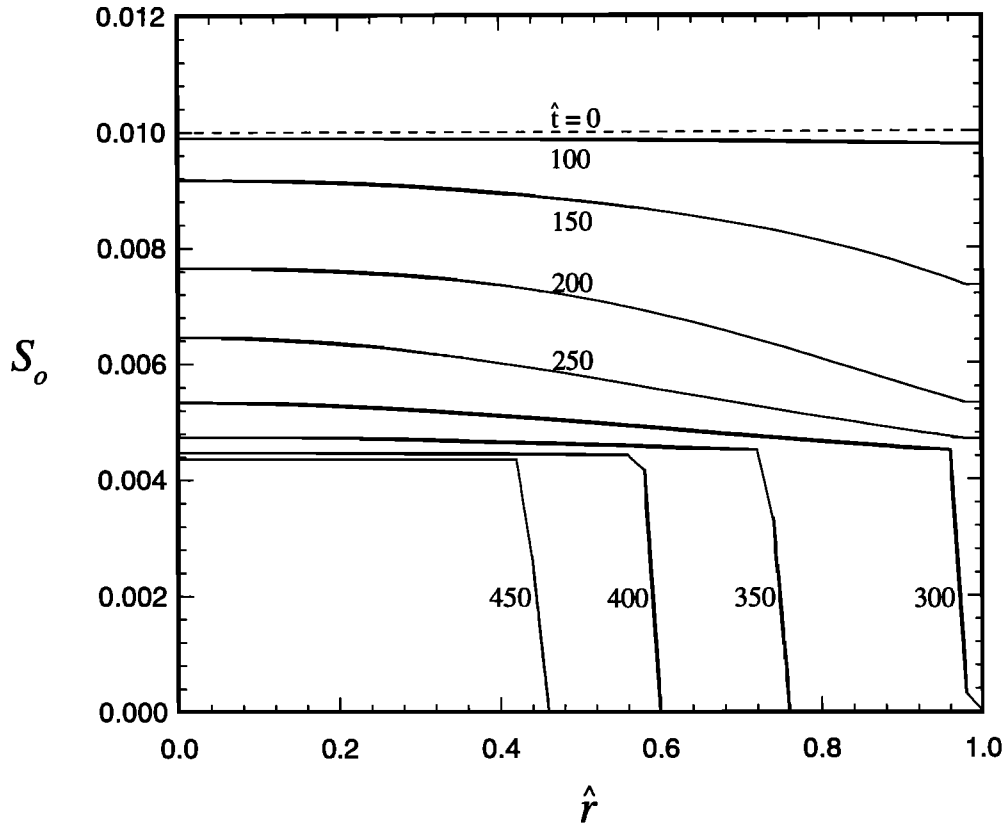


**Figure 14.** Microspatial and temporal variations of the trapped NAPL saturation $S_o$, at the macroposition $\hat{r}' = 0.25$ (middle of spill site) for case 2. The dashes denote the initial distribution.

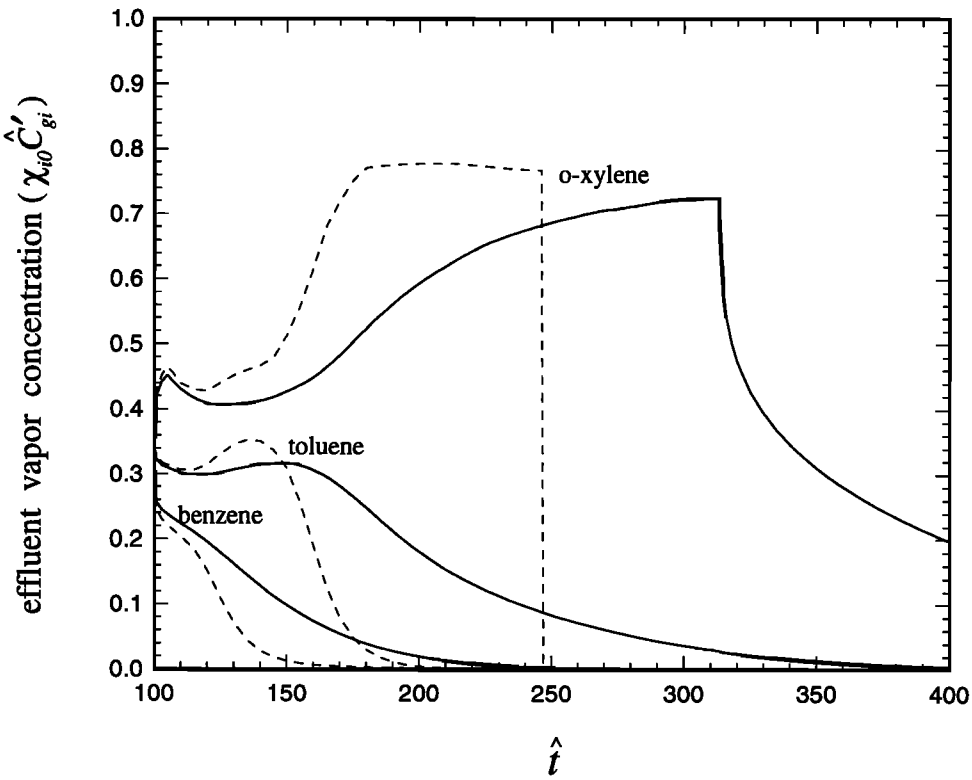


**Figure 15.** Effluent vapor concentrations for the three components in case 1 (dashes) and case 2 (solid lines).

intact core taken from a contaminated site. The predicted vapor concentrations, for both spatial distributions and effluent, have been in good agreement with the measured data for four alkanes, which are selected to represent the most volatile components in the real contaminant. The distinctive features of a multicomponent transport, namely, for a heavy component the vapor concentration may increase and has a local maximum value at the evaporation front in the course of venting, are clearly seen in both the simulation and the measured data.

The multicomponent dynamics is further studied for a horizontal and homogeneous soil layer with a radial venting into a vertical well. For a three-component NAPL composed of benzene, toluene, and o-xylene, we have found, whether or not the soil is of the aggregate type, the following distinctive behavior associated with the volatility of the components: (1) the less volatile or heavier the component is, the longer time it takes to purge this component from the soil; (2) the vapor concentration of the less volatile components can rise for some time as a result of selective evaporation of the NAPL; the rise shows up in the effluent concentrations; (3) the o-xylene vapor concentration gradient is discontinuous at the two evaporation fronts of the free NAPL, the moving speed of which can be found by a local analysis; (4) toward the final stage, the NAPL becomes virtually a pure liquid phase of o-xylene; and (5) condensation of o-xylene happens immediately downstream of the far evaporation front. The presence of trapped NAPL and soil aggregation bring about the following additional effects: (1) the clean-up time is prolonged, more for a heavier component; (2) the free NAPL is volatilized at a lower rate; (3) the rise and the subsequent fall of the o-xylene vapor concentration are much retarded; the concentration does not drop abruptly upon complete volatilization of the free NAPL; and (4) the tailing is appreciable in the effluent concentrations, a strong sign of deviation from local equilibrium. A microscale examination at the middle of the contaminated site reveals that during an intermediate stage the heavier components are fed into aggregates in response to the increase of vapor concentration in the macropores. This accumulation in trapped storage causes a longer time for these components to be removed eventually. The trapped NAPL also exhibits an inward receding front after the free NAPL at the same macroscale position is volatilized. The trapped NAPL at the core of an aggregate is, however, not removed until after a very long time of pumping.

In contrast to a first-order kinetic model which does not account for physical and chemical processes on the microscale, the present model reduces the number of fitting parameters to the minimum. While the assumption of uniform spherical aggregates may appear extreme, this idealization enables us to construct a purely deductive theory, with limited empiricism, and allows us to explain and predict many intricate phenomena from basic principles. For some manufactured materials the present theory can of course be further checked in details for both the approximations and the implications rigorously. For natural materials with irregular grains, the radius of spherical aggregates in our model can be regarded as one of the two calibrated parameters, the other being the ratio of the saturations of free and trapped NAPL. We stress that the amount of calibration, if any, required by the present model will be limited and does not increase with the number of components, as it does for a first-order kinetic model. The usefulness of the present model has been clearly demonstrated by comparison with column tests with soil samples from the field.

To further enhance the usefulness of our theory, it would be desirable to have more well-controlled experiments for a thorough comparison. In particular, we suggest a laboratory venting experiment on an unsaturated column emplaced with residual NAPL of known initial composition and total saturation. All the chemical and soil properties should be measured or estimated independently. The free and trapped NAPL saturations however may need to be calibrated using the elution curve method mentioned earlier. During venting, not only the vapor concentrations of all the components but also the NAPL saturation and composition should be measured, so that the local phase change rates predicted by the theory can be checked.

The present theory can be used for modeling more realistic configurations of air venting, where the finite length of the well screen, soil heterogeneity, ground surface conditions, and so on must be accounted for. Fully three-dimensional schemes for numerical computations are of course necessary and should be worthwhile.

**Acknowledgments.** We are grateful for funds received from the U.S. Air Force, Office of Scientific Research under grant F49620-95-1-0324, administered by Major Martin Lewis and Capt. Michael Chipley. Comments by P. Gschwend have been very helpful.

## References

Abriola, L. M., and G. F. Pinder, A multiphase approach to the modeling of porous media contamination by organic compounds, 1, Equation development, *Water Resour. Res.*, *21*(1), 11–18, 1985.

Armstrong, J. E., E. O. Frind, and R. D. McClellan, Nonequilibrium mass transfer between the vapor, aqueous, and solid phases in unsaturated soils during vapor extraction, *Water Resour. Res.*, *30*(2), 355–368, 1994.

Baehr, A. L., Selective transport of hydrocarbons in the unsaturated zone due to aqueous and vapor phase partitioning, *Water Resour. Res.*, *23*(10), 1926–1938, 1987.

Baehr, A. L., G. E. Hoag, and M. C. Marley, Removing volatile contaminants from the unsaturated zone by inducing advective air-phase transport, *J. Contam. Hydrol.*, *4*, 1–26, 1989.

Blunt, M. J., and H. Scher, Pore-level modeling of wetting, *Phys. Rev. E*, *52*(6), 6387–6403, 1995.

Blunt, M. J., D. Zhou, and D. Fenwick, Three-phase flow and gravity drainage inn porous media, *Transp. Porous Media*, *20*, 77–103, 1995.

Brusseau, M. L., Transport of organic chemicals by gas advection in structured or heterogeneous porous media: Development of a model and application to column experiments, *Water Resour. Res.*, *27*(12), 3189–3199, 1991.

Chatzis, I., N. R. Morrow, and H. T. Lim, Magnitude and detailed structure of residual oil saturation, *Soc. Pet. Eng. J.*, *23*(2), 311–326, 1983.

Corapcioglu, M. Y., and A. L. Baehr, A compositional multiphase model for groundwater contamination by petroleum products, 1, Theoretical considerations, *Water Resour. Res.*, *23*(1), 191–200, 1987.

Crow, W. L., E. P. Anderson, and E. M. Minugh, Subsurface venting of vapors emanating from hydrocarbon product on groundwater, *Ground Water Monit. Rev.*, *7*(4), 51–57, 1987.

Demond, A. H., and A. S. Lindner, Estimation of interfacial tension between organic liquids and water, *Environ. Sci. Technol.*, *27*(12), 2318–2331, 1993.

DePaoli, D. W., J. H. Wilson, and C. O. Thomas, Conceptual design of soil venting systems, *J. Environ. Eng. N. Y.*, *122*(5), 399–406, 1996.

DiGiulio, D. C., Evaluation of soil venting application, *J. Hazard. Mater.*, *32*, 279–291, 1992.

Fischer, U., R. Schulin, and M. Keller, Experimental and numerical investigation of soil vapor extraction, *Water Resour. Res.*, *32*(12), 3413–3427, 1996.

Fuller, E. N., P. D. Schettler, and J. C. Giddings, A comparison of methods for predicting gaseous diffusion coefficients, *J. Gas Chromatogr.*, *3*(7), 222–227, 1965.

Gill, S. J., N. F. Nichols, and I. Wadsö, Calorimetric determination of

enthalpies of solution of slightly soluble liquids, II, Enthalpy of solution of some hydrocarbons in water and their use in establishing the temperature dependence of their solubilities, *J. Chem. Thermodyn.*, *8*, 445–452, 1976.

Hayden, N. J., and T. C. Voice, Microscopic observation of a NAPL in a three-fluid-phase soil system, *J. Contam. Hydrol.*, *12*, 217–226, 1993.

Hayden, N. J., T. C. Voice, M. D. Annable, and R. B. Wallace, Change in gasoline constituent mass transfer during soil venting, *J. Environ. Eng. N. Y.*, *120*(6), 1598–1614, 1994.

Ho, C. K., and K. S. Udell, An experimental investigation of air venting of volatile liquid hydrocarbon mixtures from homogeneous and heterogeneous porous media, *J. Contam. Hydrol.*, *11*, 291–316, 1992.

Ho, C. K., S.-W. Liu, and K. S. Udell, Propagation of evaporation and condensation fronts during multicomponent soil vapor extraction, *J. Contam. Hydrol.*, *16*, 381–401, 1994.

Johnson, P. C., M. W. Kemblowski, and J. D. Colthart, Quantitative analysis for the cleanup of hydrocarbon-contaminated soils by in-situ soil venting, *Ground Water*, *28*, 413–429, 1990.

Kaluarachchi, J. J., and J. C. Parker, Modeling multicomponent organic chemical transport in three-fluid-phase porous media, *J. Contam. Hydrol.*, *5*, 349–374, 1990.

Leverett, M. C., Capillary behavior in porous solids, *Trans. Am. Inst. Min. Metall. Pet. Eng.*, *142*, 152–169, 1941.

Lide, D. R. (Ed.), *CRC Handbook of Chemistry and Physics*, 77th ed., CRC Press, Boca Raton, Fla., 1996.

Lingineni, S., and V. K. Dhir, Modeling of soil venting processes to remediate unsaturated soils, *J. Environ. Eng. N. Y.*, *118*(1), 135–152, 1992.

Lingineni, S., and V. K. Dhir, Controlling transport processes during NAPL removal by soil venting, *Adv. Water Resour.*, *20*(2–3), 157–169, 1997.

Mackay, D., and W. Y. Shiu, A critical review of Henry's law constants for chemicals of environmental interest, *J. Phys. Chem. Ref. Data*, *10*(4), 1175–1199, 1981.

Marley, M. C., and G. E. Hoag, Induced soil venting for recovery/restoration of gasoline hydrocarbons in the vadose zone, paper presented at NWWA/API Conference on Petroleum Hydrocarbons and Organic Chemicals in Ground Water—Prevention, Detection and Restoration, Houston, Tex., 1984.

Millington, R. J., Gas diffusion in porous media, *Science*, *130*, 100–102, 1959.

Ng, C. O., Asymptotic methods applied to the geoenvironmental problems of ground subsidence and soil vapor extraction, Ph.D., dissertation, Mass. Inst. of Technol., Cambridge, 1998.

Ng, C. O., and C. C. Mei, Homogenization theory applied to soil vapor extraction in aggregated soils, *Phys. Fluids*, *8*, 2298–2306, 1996a.

Ng, C. O., and C. C. Mei, Aggregate diffusion model applied to soil vapor extraction in unidirectional and radial flows, *Water Resour. Res.*, *32*(5), 1289–1297, 1996b.

Ostendorf, D. W., A. J. Lutenegger, and S. J. Pollock, Soil gas sampling and analysis in petroleum-contaminated transportation department right of way, *Transp. Res. Rec.*, *1475*, 110–122, 1995a.

Ostendorf, D. W., et al., Fate and transport of petroleum hydrocarbons at a leaking storage tank site, U. Mass. Transp. Cent., Amherst, 1995b.

Ostendorf, D. W., A. J. Lutenegger, R. J. Suchana, P. S. Cheever, and S. J. Pollock, LNAPL detection, measurement, and distribution in the subsurface environment, paper presented at Non-Aqueous Phase Liquids (NAPLs) in Subsurface Environment: Assessment and Remediation, Am. Soc. of Civ. Eng., Washington, D. C., 1996.

Ostendorf, D. W., D. J. DeGroot, M. M. Meyer, and S. J. Pollock, Evaporation rates and reaction kinetics of petroleum biosparging from intact core sleeves, in *Global Environmental Biotechnology*, edited by D. L. Wise, pp. 639–659, Elsevier, New York, 1997.

Parker, J. C., and R. J. Lenhard, A model for hysteretic constitutive relations governing multiphase flow, 1, Saturation-pressure relations, *Water Resour. Res.*, *23*(12), 2187–2196, 1987.

Perry, R. H., and D. Green, *Perry's Chemical Engineer's Handbook*, McGraw-Hill, New York, 1984.

Rathfelder, K., W. W.-G. Yeh, and D. Mackay, Mathematical simulation of soil vapor extraction systems: Model development and numerical examples, *J. Contam. Hydrol.*, *8*, 263–297, 1991.

Schwarzenbach, R. P., P. M. Gschwend, and D. M. Imboden, *Environmental Organic Chemistry*, Wiley-Interscience, New York, 1993.

Sleep, B. E., and J. F. Sykes, Modeling the transport of volatile organics in variably saturated media, *Water Resour. Res.*, *25*(1), 81–92, 1989.

Wilkins, M. D., L. M. Abriola, and K. D. Pennell, An experimental investigation of rate-limited nonaqueous phase liquid volatilization in unsaturated porous media: Steady state mass transfer, *Water Resour. Res.*, *31*(9), 2159–2172, 1995.

Wilson, J. L., and S. H. Conrad, Is physical displacement of residual hydrocarbons a realistic possibility in aquifer restoration? paper presented at NWWA/API Conference on Petroleum Hydrocarbons and Organic Chemicals in Ground Water—Prevention, Detection and Restoration, Houston, Tex., 1984.

Zhou, D., and M. Blunt, Effect of spreading coefficient on the distribution of light non-aqueous phase liquid in the subsurface, *J. Contam. Hydrol.*, *25*, 1–19, 1997.

C. C. Mei, Ralph M. Parsons Laboratory, Department of Civil and Environmental Engineering, Massachusetts Institute of Technology, Cambridge, MA 02139. (e-mail: ccmei@mit.edu)

C.-O. Ng, Department of Mechanical Engineering, University of Hong Kong, Pokjulam Road, Hong Kong.

D. W. Ostendorf, Department of Civil and Environmental Engineering, University of Massachusetts, Amherst, MA 01003.

(Received October 10, 1997; revised June 17, 1998;
accepted June 25, 1998.)